**ANKARA YILDIRIM BEYAZIT UNIVERSITY**

**GRADUATE SCHOOL OF NATURAL AND APPLIED SCIENCES**




# THE EFFECT OF Ni-SiC ELECTROCOMPOSITE COATING ON THE MECHANICAL PROPERTIES OF AVIATION PISTON ENGINE CYLINDERS

**M.Sc. Thesis by**

**Mehmetcan ÖKSÜZ**

**Department of Materials Engineering**

**August, 2025**

**ANKARA**

# THE EFFECT OF Ni-SiC ELECTROCOMPOSITE COATING ON THE MECHANICAL PROPERTIES OF AVIATION PISTON ENGINE CYLINDERS

**Thesis Submitted to**

**The Graduate School of Natural and Applied Sciences of**

**Ankara Yıldırım Beyazıt University**

**In Partial Fulfillment of the Requirements for the Degree of Master of Science in Materials Engineering, Department of Materials Engineering**

**by**

**Mehmetcan ÖKSÜZ**

**August 2025**

**ANKARA**

## M.Sc. THESIS EXAMINATION RESULT FORM

We have read the thesis entitled **"THE EFFECTS OF Ni-SiC ELECTROCOMPOSITE COATING ON THE MECHANICAL PROPERTIES OF AVIATION PISTON ENGINE CYLINDERS"** completed by **MEHMETCAN ÖKSÜZ** under the supervision of **PROF. DR. GÜVEN ÇANKAYA** and we certify that in our opinion it is fully adequate, in scope and in quality, as a thesis for the degree of Master of Science.

Prof. Dr. Güven ÇANKAYA

Supervisor

Doç. Dr. Begüm Ünveroğlu ABDİOĞLU

Jury Member

Prof. Dr. Hakan ATEŞ

Jury Member

Prof. Dr. İlyas ÇANKAYA

Director

Graduate School of Natural and Applied Sciences

# ETHICAL DECLARATION

I hereby declare that, in this thesis which has been prepared in accordance with the Thesis Writing Manual of Graduate School of Natural and Applied Sciences,

- All data, information and documents are obtained in the framework of academic and ethical rules,
- All information, documents and assessments are presented in accordance with scientific ethics and morals,
- All the materials that have been utilized are fully cited and referenced,
- No change has been made on the utilized materials,
- All the works presented are original,

and in any contrary case of above statements, I accept to renounce all my legal rights.

**Date: ..../...../.....** **Signature:**……...

**Name & Surname:……**

# ACKNOWLEDGMENTS

I would like to express my deepest gratitude to my advisor Prof. Dr. Güven ÇANKAYA for his invaluable guidance, constructive criticism, and continuous support throughout the course of this research. His insights and encouragement have been instrumental in the successful completion of my thesis.

This research was generously supported by EST ENDÜSTRİ TEKNİK Incorporation, to whom I would like to express my sincere appreciation for their financial and technical contributions.

I would also like to extend my special thanks to Zeliha ÖZBEK, İsmail Murat ÖZBEK, Mehmet Halim ÖZBEK, Uğur KARAHAN, Kardelen Gündoğdu ÇAĞAN, Berkay ÇAĞAN, Ebrar Sude BAŞER, and all my colleagues and friends who provided invaluable support, insightful comments, and moral encouragement throughout my academic journey.

Finally, I am deeply thankful to my family, especially my dear mother, father, and brother for their endless love, patience, and encouragement. I am also sincerely grateful to my girlfriend, whose unwavering support and affection helped me stay motivated and determined during the most challenging times of this process.

**2025, 06 August** **Mehmetcan ÖKSÜZ**

# THE EFFECT OF Ni-SiC ELECTROCOMPOSITE COATING ON THE MECHANICAL PROPERTIES OF AVIATION PISTON ENGINE CYLINDERS


## ABSTRACT

In this study, the electrolytic nickel coating process reinforced with ceramic particles was investigated in order to increase the wear resistance of cast aluminum alloy single-piston cylinders used especially in unmanned aerial vehicles (UAVs) and drones. Coating experiments were carried out in a 2-liter glass beaker using a heating magnetic stirrer; the effects of parameters such as temperature, time, current density, bath composition and pH on the thickness, hardness and ceramic dispersion of the coating were investigated. After metallographic preparation, the samples were analyzed in detail with scanning electron microscope and microhardness measurements were performed. The findings showed that a coating with a thickness of at least 70 microns was obtained with the coating process applied between 60, 75, 90 minutes at the optimized current density, the silicon carbide (SiC) content of this coating varied between 7-13% and the coating hardness ranged between 450-550 Vickers. These results indicate that the Ni-SiC electrocomposite coating provides significant wear resistance on the surface of cast aluminum alloy and offers a potential solution for improving the mechanical properties of single-piston aviation cylinders. Future studies promise more comprehensive investigations to evaluate the long-term performance of these coatings in operational conditions, both tribologically and corrosively.


**Keywords:** Single-piston aviation cylinders, cast aluminum alloy, Ni-SiC electrocomposite coating, microhardness, electrodeposition.

# HAVACILIK PİSTONLU SİLİNDİRLERİNİN MEKANİK ÖZELLİKLERİNE Ni-SiC ELEKTROKOMPOZİT KAPLAMANIN ETKİSİ

## ÖZ

Bu çalışmada, insansız hava araçları (İHA) ve dronlar gibi özellikle alüminyum alaşımlı dökme tek pistonlu silindirlerin aşınma dayanımını artırmak amacıyla seramik partiküllerle takviye edilmiş elektrolitik nikel kaplama işlemi incelenmiştir. Kaplama deneyleri, bir 2 litrelik cam beherde ısıtmalı manyetik karıştırıcı kullanılarak gerçekleştirilmiş; kaplama kalınlığı, sertlik ve seramik dağılımı üzerindeki sıcaklık, zaman, akım yoğunluğu, banyosunu bileşimi ve pH gibi parametrelerin etkisi araştırılmıştır. Metalografik hazırlığın ardından örnekler, taramalı elektron mikroskobu ile detaylı bir şekilde incelenmiş ve mikrosertlik ölçümleri yapılmıştır. Elde edilen bulgular, optimize edilmiş akım yoğunluğunda 60, 75, 90 dakika arasında uygulanan kaplama işlemi ile en az 70 mikron kalınlığında bir kaplama elde edildiğini, bu kaplamadaki silikon karbür (SiC) içeriğinin %7-13 arasında değiştiğini ve kaplama sertliğinin 450-550 Vickers arasında olduğunu göstermiştir. Bu sonuçlar, Ni-SiC elektrokompozit kaplamanın dökme alüminyum alaşımlarının yüzeyinde önemli bir aşınma direnci sağladığını ve tek pistonlu havacılık silindirlerinin mekanik özelliklerinin iyileştirilmesi için potansiyel bir çözüm sunduğunu göstermektedir. Gelecekteki çalışmalar, bu kaplamaların operasyonel koşullarda tribolojik ve korozyonel açıdan uzun dönem performanslarını değerlendirmek amacıyla daha kapsamlı araştırmalar vaat etmektedir.

**Anahtar Kelimeler:** Tek pistonlu havacılık silindirleri, dökme alüminyum alaşımı, Ni-SiC elektrokompozit kaplama, mikrosertlik, elektro kaplama.

# CONTENTS

M.Sc. THESIS EXAMINATION RESULT FORM ..... iii
ETHICAL DECLARATION ..... v
ACKNOWLEDGMENTS ..... v
ABSTRACT ..... vii
ÖZ ..... viii
NOMENCLATURE ..... xi
LIST OF TABLES ..... xivv
LIST OF FIGURES ..... xv

**CHAPTER 1-INTRODUCTION ..... 1**
1.1 The Role of Piston Engine Technologies in Aviation ..... 1
1.2 Piston Types Used in Aviation ..... 3
1.3 Coatings Used in Internal Combustion Engine Pistons ..... 4
1.4 Nickel-Based Electrochemical Coatings and Significance ..... 5
1.5 Ni–SiC Electrocomposite Coatings: A Promising Solution ..... 5

**CHAPTER 2-LITERATURE REVIEW ..... 7**
2.1 Fundamental Considerations of Electrochemistry ..... 7
2.1.1 Brief Description of Electrochemical Cell and Reactions ..... 7
2.1.2 Faradaic and Nonfaradaic Processes ..... 9
2.1.3 Kinetics and Mechanism of Electrochemical Deposition ..... 122
2.1.4 Relationships Between Electrode Potential and Thermodynamic Equilibrium ..... 13
2.1.5 Relationships Between Potential and Current ..... 15
2.2 Electrical Conductivity of the Electrolyte ..... 17
2.3 Current and Distribution of Metal on Electrode Surface ..... 18
2.4 Classification of Composite Materials ..... 19
2.5 Composite Coatings Production Methods ..... 20
2.5.1 Thermal Spraying Method ..... 21
2.5.2 Powder Metallurgy Method ..... 21
2.5.3 Electrochemical Method ..... 21
2.6 Parameters Affecting the Electrochemical Composite Coating Process ..... 25

2.6.1 Current Type and Density ..... 25
2.6.2 Working Temperature ..... 26
2.6.3 pH Value of the Plating Bath ..... 26
2.6.4 Bath Composition ..... 27
2.6.5 Stirring Rate ..... 28
2.6.6 Particle Influence ..... 28
2.6.7 Zeta Potential ..... 29
2.7 Particle Deposition Mechanism in Electrochemical Composite Coating Processes ..... 30
2.7.1 Early Models ..... 30
2.7.2 Empirical Models ..... 31
2.7.2.1 Guglielmi Model ..... 31
2.7.2.2 Kariapper and Foster Model ..... 33
2.7.2.3 Buelens and Celis Model ..... 34
2.7.2.4 Hwang and Hwang Model ..... 35
2.7.3 Advanced Models ..... 36
2.7.3.1 Valdes Model ..... 36
2.7.3.2 Guo et al. Model ..... 37
2.7.3.3 Fransaer et al. Model ..... 38
2.7.3.4 Hovestad et al. Model ..... 39
2.7.4 Ni-SiC Composite Coatings ..... 41

**CHAPTER 3-EXPERIMENTAL PROCEDURE ..... 44**
3.1 Preparation of Nickel-SiC Electrocomposite Bath ..... 44
3.2 Base Material Selection And Sample Preparation ..... 45
3.3 Nickel-SiC Electrocomposite Coating Study ..... 46
3.3.1 Ni-SiC Composite Coating Experiments ..... 47
3.4 Characterization Studyies ..... 48
3.4.1 X-Ray Diffraction (XRD) Analysis ..... 48
3.4.2 Hardness Measurements ..... 49
3.4.3 CSM-Tribometer ..... 50
3.4.4 SEM-EDS Analyses ..... 51

**CHAPTER 4-RESULTS AND DISCUSSION ..... 52**

4.1 Effect of Deposition Time and Temperature on Coating Thickness ..... 52
4.2 Microstructural Analysis of Ni–SiC Coatings ..... 53
4.3 Influence of SiC Concentration and Current Density ..... 60
4.4 Tribological Behavior of Ni–SiC Coatings ..... 64
4.5 Structural Phase Analysis via XRD ..... 67

**CHAPTER 5-CONCLUSION ..... 72**
**REFERENCES ..... 74**
**CURRICULUM VITAE ..... 81**

# NOMENCLATURE

## Roman Letter Symbols

| | |
|---|---|
| $A$ | Surface area, $dm^2$ |
| $C_0$ | Bulk concentration, mole/$cm^3$ |
| $C_b$ | Concentration of metal ion |
| $C_{eff}$ | Current efficiency, % |
| $D$ | Diffusion coefficient |
| $E$ | Potential, V |
| $E^{\circ}_{cell}$ | Reversible standard cell potential, V |
| $E_{iR}$ | Ohmic drop |
| $F$ | Faraday's constant, C/mole |
| $G$ | Gibbs free energy |
| $G$ | Conductance, Siemens |
| $I$ | Current, ampere |
| $K_{eq}$ | Equilibrium constant |
| $L$ | Thickness of diffusion layer |
| $M$ | Molecular weight of the deposited metal, grams/mole |
| $N_A$ | Avogadro's number, molecules/mole |
| $Q$ | Transferred charge, ampere.second |
| $Q_R$ | Number of coulombs needed for reaction |
| $Q_T$ | Total number of coulombs passed through the cell |
| $R$ | Gas constant |
| $R$ | Ohmic resistance, Ω |
| $R_C$ | Compensated resistance |
| $R_s$ | Resistance of electrolyte solution |
| $R_U$ | Uncompensated resistance |

| | |
|---|---|
| $T$ | Temperature, Kelvin |
| $T$ | Thickness, cm |
| $W_{actual}$ | Weight of deposited metal actually, grams |
| $W_{theoretical}$ | Theoretical weight of deposited metal, grams |
| $a_c$ | Constant for cathodic process |
| $b_c$ | Constant for cathodic process |
| $d$ | Density, gram/cm$^3$ |
| $e$ | Charge of electron, C |
| $i$ | Current density, ampere/dm$^2$ |
| $i_0$ | Exchange current density |
| $i_L$ | Limiting current density |
| $i_p$ | Peak current, ampere |
| $i_{p,a}$ | Anodic peak current, ampere |
| $i_{p,c}$ | Cathodic peak current, ampere |
| $n$ | Number of valance electrons |
| $q$ | Charge, C |
| $t$ | Duration, second |
| $w$ | Weight of the metal deposited, grams |
| $z$ | Number of electrons |
| $\Delta E_p$ | Peak–to–peak separation |
| $\Delta G$ | Change in gibbs free energy of the reaction, J/mole |
| $\Delta G^\circ$ | Standard gibbs free energy, J/mole |
| $\Delta G^\circ_{298}$ | Formation of gibbs free energy, J/mole |

**Greek Letter Symbols**

| | |
|---|---|
| $\alpha$ | Transfer Coefficient |
| $\nu$ | Scan rate, mV/second |

| | |
|---|---|
| $\eta_a$ | Anodic Overpotential, V |
| $\eta_c$ | Cathodic Overpotential, V |
| $\Delta$ | Difference |

**Acronyms**

| | |
|---|---|
| COF | Coefficient of Friction |
| EDS | Energy–Dispersive X–Ray Spectroscopy |
| OCP | Open Circuit Potential |
| SEM | Scanning Electron Microscope |
| SiC | Silicone Carbide |
| XRD | X-Ray Diffraction |

# LIST OF TABLES

**Table 1.1** Comparison of Galvanic and Electrolytic Cells in Faradaic Processes ..... 11
**Table 2.1** Comparison of Composite Coating Models ..... 40
**Table 3.1** Composition of the Nickel-SiC Electrocomposite Coating Bath ..... 45
**Table 3.2** Parameters and Levels for Ni-SiC Composite Coating Experiments ..... 48

# LIST OF FIGURES

**Figure 1.1** A front view of the TEI-PG50 two-stroke boxer-type piston engine developed for UAV applications ..... 2

**Figure 2.1** Illustration of an electrolytic (electrodeposition) cell. Reproduced from . 8

**Figure 2.2** Helmholtz (or Stern) electrical double layer model. Reproduced from.. 10

**Figure 2.3** Two types of electrochemical cells for faradaic process: a) Galvanic cell, b) Electrolytic cell. Reproduced from ..... 11

**Figure 2.4** Example of non-homogeneous thickness distributions and highest current density areas. Reproduced from ..... 19

**Figure 2.5** Electrolysis system used in the production of electroplated composite coatings ..... 23

**Figure 2.6** Particle incorporation mechanism into metal coating according to the Buelens ..... 35

**Figure 2.7** Forces acting on a particle; Ff: frictional force, Fa: adhesion force, and Fd: detachment force attempting to remove the particle ..... 38

**Figure 2.8** Zinc coating growth morphologies: (a)irregular, (b) parallel, and (c) vertically hexagonal plates, where black represent coated particles ..... 39

**Figure 2.9** Schematic Representation of a Ni-SiC Composite Coating ..... 42

**Figure 3.1** Pre-treatment steps for aluminum substrate. ..... 46

**Figure 3.2** Experimental setup where the coating processes were carried out..... 47

**Figure 3.3** D8 Advance XRD device..... 49

**Figure 3.4** Fischer HP100 X-Y PROG brand ultra microhardness device..... 50

**Figure 3.5** CSM Tribometer brand wear device assembly..... 51

**Figure 3.6** JEOL JSM-6060LV Scanning Electron Microscope used for the morphological and cross-sectional characterization of Ni-SiC composite coatings. . 51

**Figure 4.1** Variation of coating thickness (μm) as a function of coating time (min) for different current densities (2.5, 5, and 10 A/dm²) under constant temperature (55 °C) and pH 4.0 and 0,40 g/L SiC ..... 52

**Figure 4.2** Variation of coating thickness (μm) as a function of bath temperature (°C) for different deposition times (60, 75, and 90 minutes) at constant current density (10 A/dm²) and pH 4.0 and 0,40 g/L SiC. ..... 53

**Figure 4.3** Same sample A and A1 both coated under 4 pH 55 °C 75 min 0,40g/L SiC 2.5 A/dm² current density. ..... 54

**Figure 4.4** EDS spectra of Sample A (top) and Sample B (bottom), revealing the elemental composition of the Ni–SiC coatings. ..... 54

**Figure 4.5** Same sample B and B1 both coated under 4 pH 55 °C 75 min 0,40g/L SiC 5 A/dm² current density. ..... 56

**Figure 4.6** EDS spectra of Sample C (top) and Sample D (bottom), revealing the elemental composition of the Ni–SiC coatings. ..... 57

**Figure 4.7** Same sample C and C1 both coated under 4 pH 55 °C 75 min 0,40g/L SiC 10 A/dm² current density..... 58

**Figure 4.8** Figure 4.8: EDS spectra of Sample C (top) and Sample C1 (bottom), revealing the elemental composition of the Ni–SiC coatings.. ..... 59

**Figure 4.9** Effect of SiC concentration on coating thickness at different current densities..... 60

**Figure 4.10** Variation of coating thickness (μm) as a function of current density (A/dm²) for different deposition times (60, 75, and 90 minutes). Bath temperature and SiC particle concentration were fixed at 55 °C and 40 g/L, respectively..... 61

**Figure 4.11** Effect of SiC concentration and current density on the microhardness (HV) of Ni–SiC composite coatings ..... 62

**Figure 4.12** Change in SiC incorporation in Ni-SiC coatings as a function of bath SiC concentration and current density ..... 63

**Figure 4.13** Real-time friction coefficient (μ) variation with sliding distance for Ni–SiC coatings deposited at 2,5 A/dm² using an alumina counter ball. Both samples A were coated under identical conditions: pH 4.0, 55 °C, 75 min, 0.40 g/L SiC..... 64

**Figure 4.14** Real-time friction coefficient (μ) variation with sliding distance for Ni–SiC coatings deposited at 5 A/dm² using an alumina counter ball. Both samples B were coated under identical conditions: pH 4.0, 55 °C, 75 min, 0.40 g/L SiC.. ..... 65

**Figure 4.15** Real-time friction coefficient (μ) variation with sliding distance for Ni–SiC coatings deposited at 10 A/dm² using an alumina counter ball. Both samples C were coated under identical conditions: pH 4.0, 55 °C, 75 min, 0.40 g/L SiC..... 66

**Figure 4.16** XRD pattern of SiC ceramic powder (JCPDS No: 01-073-1663)..... 67

**Figure 4.17** XRD pattern of Ni/SiC coating deposited at 2.5 A/dm² for 75 min, showing dominant Ni peaks (JCPDS No: 01-071-4655) with no distinct SiC peaks (JCPDS No: 01-073-1663)..... 68

**Figure 4.18** XRD pattern of Ni-SiC coating obtained at 5 A/dm² for 75 minutes, showing peaks of Ni, SiC, and possible $Ni_3Si$ phases..... 69

**Figure 4.19** XRD pattern of Ni-SiC coating obtained at 10 A/dm² for 75 minutes, showing distinct peaks of Ni and SiC phases (JCPDS No: 01-071-4655 and 01-073-1663). ..... 70

**Figure 4.20** Comparison of XRD patterns of Ni-SiC coatings deposited at 2.5, 5, and 10 A/dm² for 75 minutes. Increased current density enhances the visibility of SiC peaks..... 71

# CHAPTER 1

## INTRODUCTION

### 1.1 The Role of Piston Engine Technologies in Aviation

Since the early days of powered flight, piston machines have played a central part in the development of aeronautics. [1]. Although the ultramodern aerospace assiduity has extensively espoused gas turbine machines for marketable and military aircraft due to their high thrust- to- weight rate and effectiveness at high mound, internal combustion piston machines remain necessary in several sectors of aeronautics [2]. These machines are especially current in light aircraft, unmanned upstanding vehicles (UAVs), gliders, flight training aircraft, and homebuilt experimental aeroplanes.

One of the primary advantages of piston machines in aeronautics is their mechanical simplicity and ease of conservation. In discrepancy to the complexity and cost of turbine- grounded propulsion systems, piston machines are cost-effective, robust, and fluently fixable, making them particularly seductive for operations where budget constraints, cargo capacity, or low- altitude operation are significant factors [1].

Moreover, developments in composite coatings, materials science, fuel injection systems, electronic engine management, and fuel injection systems have revived the importance of piston engines in aviation uses [3]. Even under trying flight conditions, modern piston engines can deliver high power-to-weight ratios, better thermal efficiency, and greater dependability. Their capability to work effectively at low to medium altitudes and to run on Aviation Gasoline (AVGAS) or alternative fuels strengthens their usefulness in unique operations like surveillance, aerial mapping, border patrol, and agricultural spraying, for which turbine engines would be economically or technically impossible [2].

Apart from fixed-wing aircraft, piston engines are also commonly found in rotorcraft (small helicopters and gyrocopters), Remotely Piloted Aircraft Systems (RPAS), particularly in military and research settings [2]. Particularly with the advent of UAVs

and hybrid-electric aircraft ideas, piston engines keep changing as demand for light and effective propulsion systems rises, and they are using modern materials as well as surface engineering techniques to improve their mechanical properties and longevity [3]. A representative image of the TEI-PG50 piston engine developed for UAV applications is presented in Figure 1.1.

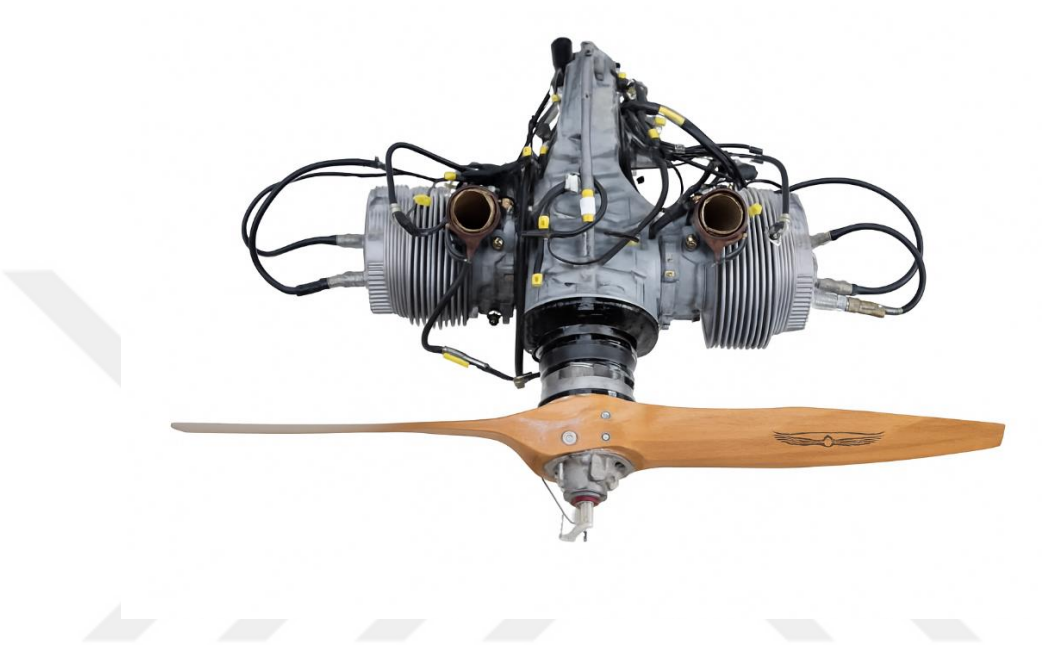

**Figure 1.1** A front view of the TEI-PG50 two-stroke boxer-type piston engine developed for UAV applications [6].

In this light, it is rather more important to improve the performance and lifespan of cylinder and pistons, which under severe thermal, mechanical, and tribological stresses. Particularly experiments in surface engineering including sophisticated electrocomposite coatings, provide exciting answers to these problems [4][5]. Ultimately lengthening the service life and operational safety of aviation piston engines, the employment of such coatings might greatly improve wear resistance, corrosion protection, and general engine performance.

## 1.2 Piston Types Used in Aviation

Pistons are employed in internal combustion engines to transform combustion energy into mechanical motion. High temperatures, high pressure loads, cyclic reciprocating motion, and high frequency vibration are all challenges that piston aviation must withstand [3]. For the engine to be dependable, quick, and safe, design and material choices are essential.

Steel-based alloy pistons are typically used in high-performance examples of aerospace piston engines but are commonly made of lightweight aluminum alloys. The aluminum - silicon alloys are greatly preferred due to low weight with high heat conductance. The pistons are surface hardened or coated with harder, heat-resistant material to increase their strength against wear and heat, although they are not very strong under high temperatures [5]. Aviation pistons are generally classified as follows:

Monolithic pistons are prevalent in general aviation due to mechanical strength and simple manufacturing practices. Segmented pistons or composite pistons are used to combine materials with dissimilar characteristics and are most frequently structured with a steel crown to resist heat and an aluminum skirt for lightness. They are used under heavy loads where thermal gradients occur within the components. Slipper pistons are reduced in overall weight and friction and machined. Engines that focus on mass and efficiency tend to have low reciprocating motion. Full-skirt pistons are structurally stiffer and are best appropriate to engines with long stroke length or lateral forces. The configuration of a piston is affected primarily by thermal expansion behavior, lubrication control, and combustion chamber contour. For example, cam-mounted pistons are of oval shape to accommodate thermal expansion under running conditions. Cool pistons with oil galleries for internal cooling are also commonly used in aviation engines with higher compression ratios.Piston design is significantly influenced by combustion chamber form, lubrication control, and thermal expansion properties [3].

For example, cam-mounted pistons are oval in shape to accommodate for thermal expansion when operating. In aircraft engines of increased compression ratio, cooled pistons with internal oil galleries for cooling are also becoming increasingly popular.

The piston face is generally composed of three main areas:

1. Crown: upper surface exposed directly to combustion; must be able to endure wear, oxidation and thermal fatigue.

2. Piston ring clearance: critical for the control of oil consumption and sealing.

Skirt: side piece that keeps things in line and reduces friction in the cylinder.

Since these regions face various mechanical, thermal and friction problems, they require specific surface treatments or coatings to improve performance and extend their lifespan [4,5].

## 1.3 Coatings Used in Internal Combustion Engine Pistons

Pistons in internal combustion engines must withstand severe service conditions such as high temperature, severe combustion gases and constant friction. These rough surroundings regularly cause structural failure, wear, rust, and thermal fatigue. Surface coatings are added to improve the performance and longevity of piston components to counteract these results [7].

By lowering friction, improving corrosion resistance, adding thermal insulation, and keeping dimensional stability under cyclic loads, coating helps maintain dimensional stability under cyclic loads. Usually used coverings are:

-Hard chrome plates for wear resistance.
-Using ceramics like YSZ for thermal insulation, Thermal Barrier Coatings (TBCs) would be developed.
-Coatings meant for low friction and chemical resistance with TiN or DLC (Diamond Like Coating) are based on Physical Vapor Deposition (PVD) and Chemical Vapor Deposition (CVD).
- Self-lubrication composite coatings of graphite or $MoS_2$ [8]

Though they have advantages, these coatings can fail under fast loads via delamination or brittle fracture. As a result, recent studies have given attention to electrochemical composite coating, especially nickel-based systems that provide a balance of durability, mechanical strength, and heat resistance [9].

## 1.4 Nickel-Based Electrochemical Coatings and Significance

The corrosion resistance, good adhesion and ease of deposition of nickel-based coatings make them more popular industrially. Therefore, many industries use electroplated nickel coatings to improve surface hardness and wear resistance. Their capacity to create homogeneous layers on intricate geometries at comparatively low processing temperatures makes them especially useful [10]. Electrocomposite coatings, which include hard ceramic particles into a nickel matrix, significantly improve physical characteristics like hardness, abrasion resistance, and thermal stability. Particle size, current density, and bath composition are important parameters in the electrochemical deposition processes used to create the coatings [11]. Because of their exceptional mechanical properties, nickel composites reinforced with SiC, $AlO_3$, or WC are appropriate for high-load components like cylinders and pistons in the aircraft industry [12].

## 1.5 Ni–SiC Electrocomposite Coatings: A Promising Solution

The ductility of nickel and the hardness and thermal stability of silicon carbide (SiC) combine to form a strong surface layer that can withstand the harsh operating conditions of aviation piston engines [13].

SiC particles enhance oxidation behavior, wear resistance, and microhardness. The homogeneous distribution of SiC in the Ni matrix is crucial for the electrochemical deposition of the films. The quality and performance of the coating, process parameters such as temperature, agitation speed, current density, and bath pH determine the coating optimization [14]. Quality and performance of the coating are determined by process parameters including temperature, agitation speed, current density, and bath pH [14].

According to research, Ni–SiC coatings are superior to conventional coatings against wear resistance and corrosion protection, particularly under cyclic thermal conditions. Increased service life, lower maintenance costs, and improved safety are the benefits of their use in aviation piston engine cylinders [15]. To characterize improvements in material property enhancement of coating processing and optimize it, this thesis investigates the impact of Ni–SiC electrocomposite coatings on the mechanical properties of aviation piston engine cylinders.

# CHAPTER 2

# LITERATURE REVIEW

## 2.1 Fundamental Considerations of Electrochemistry

Electrochemistry is a specialized branch of chemistry that focuses on the relationship between electricity and chemical processes [16]. A significant portion of this field involves investigating chemical reactions facilitated by the flow of electrical current and the production of electricity as a result of these reactions. The process of forming a metallic layer on a substrate through reduction reactions in an electrochemical cell is referred to as electrodeposition, also known as electroplating. Additionally, electrodeposition includes techniques such as metal extraction, known as electrometallurgy, and electroforming.

### 2.1.1 Brief Description of Electrochemical Cell and Reactions

An electrochemical cell comprises of three fundamental components: the anode, cathode, and electrolyte, as portrayed in Figure 2.1. The electrochemical responses put at the anodes, either in a reasonable fluid arrangement or liquid salt, with the association between the anode and cathode encouraged by an electrical conductor in a galvanic cell or a control source in an electrolytic cell to empower the stream of current. In an electrolytic cell, the cathode, where the diminishment response happens, is associated to the negative terminal, whereas the anode, where oxidation happens, is connected to the positive terminal of the control source. Charges are exchanged through two particular ways within the electrochemical cell:one by the stream of electrons from the anode to the cathode, and the other through the movement of particles within the electrolyte. Terminals can be either dissolvable (such as nickel, copper, or gold) or insoluble (such as platinized titanium, stainless steel, or graphite). The electrolyte, ordinarily a fluid arrangement containing ionic species, is chosen for its tall electrical conductivity [17]. The choice of a conductive or low-resistance electrolyte is basic because it impacts key electrodeposition parameters, counting connected potential, electrical effectiveness, and the quality of the store.

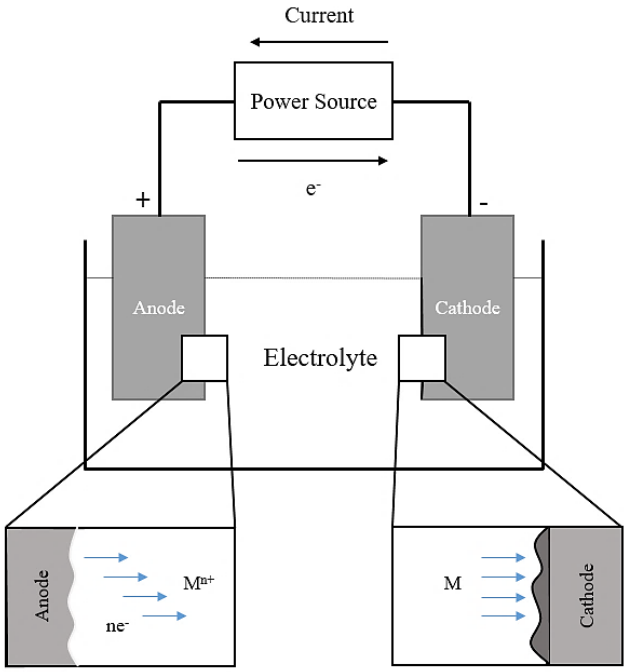


**Figure 2.2** Illustration of an electrolytic (electrodeposition) cell. Reproduced from [18]

During the electrochemical process, two types of reactions occur at the electrodes: oxidation and reduction. Once the electrochemical process begins, an equilibrium is established between the metal and its ions in the electrolyte, as represented by Eq. (2.1):

$$M^{n+} + ne^- \leftrightarrow M \tag{2.1}$$

In this context, *n* represents the number of electrons, M is the metal, and $M^{n+}$ denotes the metal ion. Reactions that involve the consumption of electrons are known as reduction reactions, while reactions that produce electrons are called oxidation reactions.

The potential differences (or Galvani potential difference) in an electrochemical cell cannot be directly measured between the electrodes experimentally, as the solution potential cannot be determined without introducing an additional metal/electrolyte interface [19]. This cell potential arises from the potential differences between the metal and the solution and is measured in volts (V), where 1 V = 1 J/C (joule per coulomb).

### 2.1.2 Faradaic and Nonfaradaic Processes

There are two different types of processes that occur at the electrodes. Typically, the electrons are transferred at the interface of the metal solution. The transfer of these electrons causes the reduction and oxidation reactions. Because these reactions are taken by Faraday's occurrence according to Faraday's law, these phenomena are referred to as faradaic called Faraday processes (or charge-transfer charge transfer electrodes). At the interface between the electrode and the solution, other processes are involved, such as adsorption and desorption, which change with the potential or composition of the solution. This is called the nonfaradaic process.

If there is no electron transfer at the interface between the electrode and the metal solution, even if potential is applied to the system from an external source, this electrode is called an Ideal Polarized Electrode (IPE). The metal solution interface may be associated with a capacitor if the electrons cannot be located around the IPE interface. The capacity can be described as a circuit component comprising two metal sheets separated by dielectric materials, and the capacitance can be calculated as:

$$C = \frac{q}{E} \tag{2.2}$$

where $C$ is the capacitance in Farad (F), $q$ is the charge in coulombs (C), and $E$ is the potential of capacitor in volts (V).

If there are potential differences in the electrochemical cell, there are Mn+ ions at the interface with the metal solution. Some of these ions are left in the solution from the metals and the remaining ions are re-entered from the metal crystal from the solution. This situation causes a charge to form on the metal-solution interface, either negatively or positively. Charging these ions involves a new configuration on the metal side and at the interface between the metal and solution. Therefore, on the solution side, several layers form, and this formation is called the electrical double layer. There are different types of models for illustrating layers similar to capacitors [20]. An example of an electric double-layer model is the Helmholtz or Stern double-layer shown in Figure

2.2.

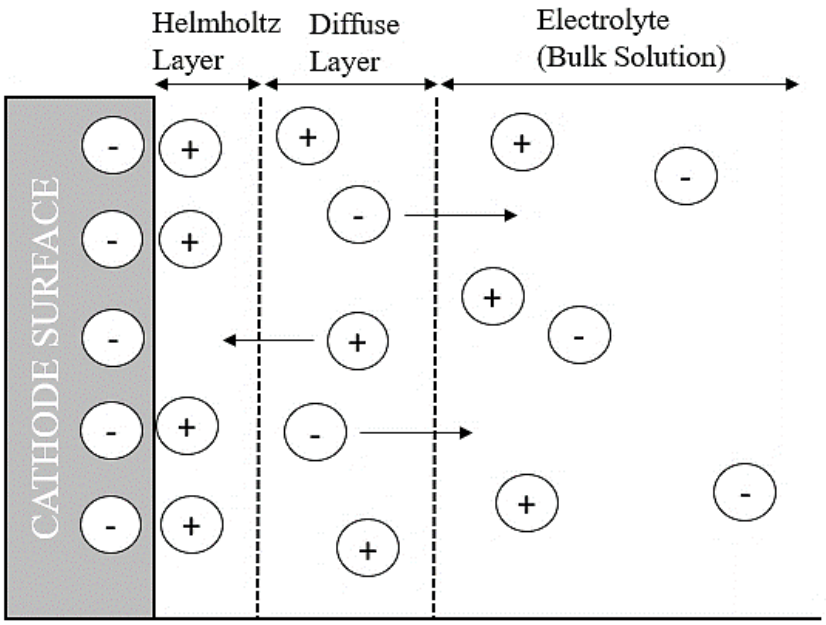


**Figure 2.3** Helmholtz (or Stern) electrical double layer model. Reproduced from [21]

There are two different types of electrochemical cell for faradaic process. Galvanic cells produce electrical energy from chemical energy. Reactions in a galvanic cell are carried out spontaneously by means of a conductor, as shown in Figure 2.4. Since total Gibbs free energy of the reaction (ΔG) is lower than zero, the system does not require an external power supply. Electrons are passed from the negative side (anode) to positive side (cathode) of the cell. Examples of the galvanic cell are primary (or nonrechargeable) cells (such as Zn-$MnO_2$ cell), secondary (or rechargeable) cells (such as a charged Pb-$PbO_2$ storage battery) and fuel cells (such as $H_2$-$O_2$ cell) [22]. Electrolytic cells do not produce electrical energy since total Gibbs free energy of the reaction is greater than zero, which means that the reaction does not occur spontaneously; therefore, this system needs an external power supply to enable the reaction. In all types of cells, oxidation and reduction reactions occurs at anode and cathode, respectively.

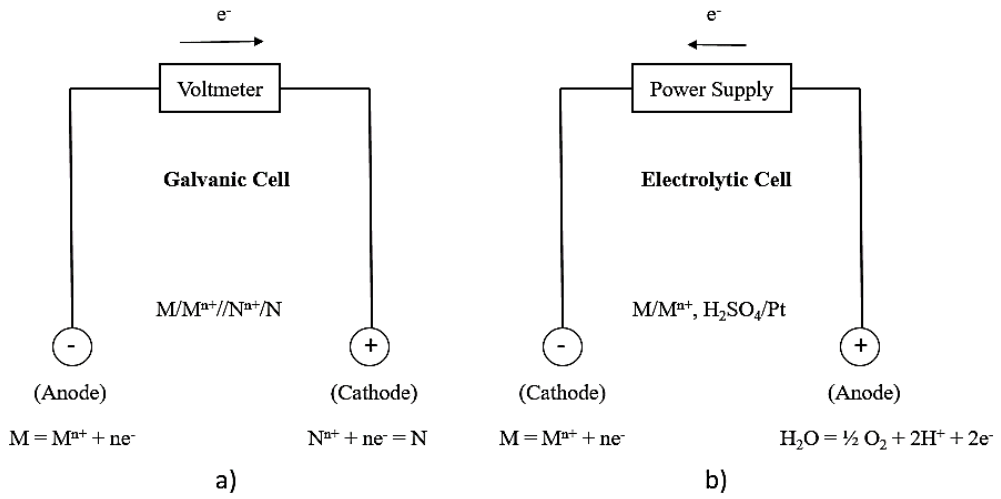


**Figure 2.4** Two types of electrochemical cells for faradaic process: a) Galvanic cell, b) Electrolytic cell. Reproduced from [23]

**Table 1.1.** Comparison of Galvanic and Electrolytic Cells in Faradaic Processes

| Feature | Galvanic Cell | Electrolytic Cell |
|---|---|---|
| Electron Flow Direction | From anode (–) to cathode (+) | From power supply to cathode (–) |
| Energy Type | Produces electrical energy | Consumes electrical energy |
| Reaction Spontaneity | Spontaneous ($\Delta G < 0$) | Non-spontaneous ($\Delta G > 0$) |
| External Power Requirement | Not required | Required (DC power source) |
| Application Example | Batteries ($Zn–MnO_2$, Pb–acid) | Electroplating (e.g., Ni–SiC coatings) |
| Anode Reaction | Oxidation ($M \rightarrow M^{n+} + ne^-$) | Oxidation (e.g., $H_2O \rightarrow O_2 + 2H^+ + 2e^-$) |
| Cathode Reaction | Reduction ($M^{n+} + ne^- \rightarrow M$) | Reduction (e.g., $Ni^{2+} + 2e^- \rightarrow Ni$) |
| Polarity of Electrodes | Anode (–), Cathode (+) | Anode (+), Cathode (–) |

*Note: In this thesis, the electrolytic cell structure was used to deposit nickel and co-deposit SiC particles onto aluminum substrates under applied current.*

### 2.1.3 Kinetics and Mechanism of Electrochemical Deposition

When the current passes through the cell, the charge is transferred from the anode to the cathode, thus depositing one atom of the metal on the cathode. Depositing one mole of metal needs

$$F = N_A . e \tag{2.3}$$

coulombs of electricity, where $N_A$ is the Avogadro's number (6.022 x $10^{23}$ molecules/mole), $e$ is the charge of an electron (1.6021 x $10^{-19}$ C) and $F$ is the Faraday's constant (96485 C/mole).

The transferred charge ($Q$) between electrons can be described as product of current ($I$) in ampere and duration ($t$) in second:

$$Q = I . t \tag{2.4}$$

As stated in the equation above, current is determined using the process's current density value in addition to the relationship with the electron's transferred charge. In electrochemistry, current density ($i$) is the ratio of the current ($I$) flowing through the cell in amperes to the electrode's surface area (A), which is typically expressed in $dm^2$.

$$i = \frac{I}{A} \tag{2.5}$$

According to Faraday's law, the weight of the metal deposited ($w$) in grams can essentially be determined.

$$w = \frac{M . I . t}{z . F} \; x \; C_{eff} \tag{2.6}$$

where $M$ is the deposited metal's molecular weight in gram/mole, $z$ is the number of

electrons in the reaction, and $C_{eff}$ is the process's current efficiency. Furthermore, the thickness of the deposit can be computed using the volume of the deposited layer. Surface area ($A$) in cm$^2$ times thickness ($T$) in cm is the product of volume. The deposited layer's thickness can be determined using the Eq. (2.7):

$$T = \frac{w}{d.A} \tag{2.7}$$

where $d$ is the metal's deposited density expressed in g/cm$^3$. Additionally, Eq. can be used to determine how long the electrodeposition process will take. (2.6). The process's current efficiency ($C_{eff}$) can be computed using two formulas. The ratio of the total number of coulombs passed through the cell ($Q_T$) to the number of coulombs required for the reaction ($Q_R$) is the first way to express current efficiency [24]:

$$C_{eff} = \frac{Q_R}{Q_T} \tag{2.8}$$

The ratio of the actual weight of deposited metal ($W_{actual}$) to the theoretical weight of deposited metal ($W_{theoretical}$), which is determined using Faraday's law, is the second method of calculating current efficiency.

$$C_{eff} = \frac{W_{actual}}{W_{theoretical}} \tag{2.9}$$

### 2.1.4 Relationships Between Electrode Potential and Thermodynamic Equilibrium

One of the thermodynamic properties is Gibbs free energy ($G$). The energy differences between products and reactants at constant temperature and pressure are what constitute the change in the system's Gibbs free energy ($\Delta G$). The following represents the change in the Gibbs free energy for a chemical reaction.

$$\Delta G = \Delta G^{\circ} + RTlnQ \tag{2.10}$$

where $Q$ is the reaction quotient, $R$ is the gas constant, $T$ is the temperature, and $\Delta G^{\circ}$ is the standard Gibbs free energy. The Gibbs free energy changes by zero at equilibrium. As a result, the standard Gibbs free energy change can be expressed as follows.

$$\Delta G^{\circ} = -RTlnK_{eq} \tag{2.11}$$

where the equilibrium constant is $K_{eq}$. Chemical reactions can be generally described as follows.

$$aA + bB = cC + dD \tag{2.12}$$

The equilibrium constant can be found using the ratio of reactant and product activities, as shown in the following equation.

$$K_{eq} = \frac{[(a_C)^c .(a_D)^d]}{[(a_A)^a .(a_B)^b]} \tag{2.13}$$

Furthermore, the electric work for the reaction can be used to calculate the change in the standard Gibbs free energy. The energy for chemical reactions serves as the driving force in an electrochemical cell. These energies can be linked to electrochemical cell potential and are derived from oxidation and reduction reactions. Consequently, $\Delta G^{\circ}$ can also be expressed as,

$$\Delta G^{\circ} = W_{electric} = -nF E^{\circ}_{cell} \tag{2.14}$$

where $E^{\circ}_{cell}$ is the reversible standard cell potential and n is the number of electrons participating in the electrochemical reaction. The electrochemical cell

potential calculation equation can be expressed as follows if the $\Delta G$ is rearranged.

$$E_{cell} = E^{\circ}_{cell} - \frac{RT}{nF} lnK \quad (2.15)$$

It's known as the Nernst equation. One possible rewrite of this equation is:

$$E_{cell} = E^{\circ}_{cell} - \frac{0.0592}{n} logK \quad (2.16)$$

The electromotive force between two electrodes is the term used to describe the total cell potential [25]. The sum of the half-cell potential of the oxidation and reduction reactions is the total cell potential.

$$E_{cell} = E_{ox.} + E_{red.} \quad (2.17)$$

The spontaneous reactions take place at $\boldsymbol{E_{cell}} > 0$ and $\boldsymbol{\Delta G} < 0$, based on the relationship between standard cell potential and change in total Gibbs free energy. There are non-spontaneous reactions when $\boldsymbol{\Delta G} > 0$ and $\boldsymbol{E_{cell}} < 0$. There is no reaction between the electrodes when $\boldsymbol{E_{cell}} = \boldsymbol{\Delta G} = 0$ and the equilibrium state is formed.

### 2.1.5 Relationships Between Potential and Current

Cell potential is different from equilibrium potential when current flows through electrodes. A cathodic (negative) shifting will make the reduction reaction the dominant one. When shifting in the anodic (positive) direction, however, the oxidation reaction becomes crucial. The following formulas provide the formulation of this shifting, which is known as the overpotential ().

$$\eta = \left| E - E_{cell} \right| \quad (2.18)$$

The overpotential of an electrochemical process in an industrial setting can range from mV to more than 2 V. Thus, the structure and quality of the

deposition may be impacted by this discrepancy. According to reports, high overpotential can result in a finer-grained structure [26]. To accomplish metal deposition, more cathodic potentials must typically be applied than the equilibrium potential. However, when the deposited atoms have a strong affinity for the substrates, applying negative potentials is not always necessary. Underpotential deposition is the term used to describe this circumstance [27].

According to Eq., current density varies exponentially with η for both large negative and positive overpotential values. Eq. and (2.19). (2.20), in that order [28].

$$i = -i_0 . e^{-a.z.f.\eta} \tag{2.19}$$

$$i = -i_0 . e^{-(1-a).z.f.\eta} \tag{2.20}$$

where $a$ is the transfer coefficient, $z$ is the number of electrons, $f$ can be computed using the following equation, and $i_0$ is the exchange current density, which is the current when the overpotential is zero.

$$f = \frac{96487\ {}^{C}/_{mol}}{\left(8.3144\ {}^{J}/_{K}\right) x\ (298\ K)} = 38.94 \frac{C}{J} = 38.94\ V^{-1} \tag{2.21}$$

where T is the absolute temperature (298 K), R is the gas constant (8.3144 J/K), and F is the Faraday's constant (96487 C. mol-1).

The Tafel equation for overpotential is the result of taking the logarithms of the current density equations for large negative and positive overpotential [29]:

$$\eta = a \pm b . log \left| i \right| \tag{2.22}$$

where the anodic and cathodic processes are denoted by the ± sign, and a and b are constants. The following equations can be used to determine the constants a and b for

cathodic processes ($a_c$ and $b_c$).

$$a_c = \left(2.303\frac{RT}{azF}\right) x \log(i_0) \tag{2.23}$$

$$b_c = (2.303\ \frac{RT}{azF}) \tag{2.24}$$

There is a limit to the relationship between current and potential, and it has to do with the transfer of $M^{n+}$ during the deposition process. The following equation can be used to calculate the limiting current density ($i_L$), which is the limit at which there is no increase in current even when additional potentials are applied to the system [30].

$$i_L = \left(\frac{nFD}{L}\right) x\ C_b \tag{2.25}$$

where $L$ is the diffusion layer thickness, $C_b$ is the $M^{n+}$ concentration, and $D$ is the diffusion coefficient.

## 2.2 Electrical Conductivity of the Electrolyte

Electrical conductivity of the electrolyte is based on concentration and motion of the ions. Measurement of conductivity is crucial for electrodeposition processes because conductivity affects the current density, and thus, metal distribution on cathode surface. Each solution has different conductivity values since specific composition can vary for each solution, for example cyanide copper, zinc and their solutions have conductivities between 6-16 $Ohm^{-1}m^{-1}$ [31]. In addition, conductivity depends on the existence of impurities and gas bubbles. If it is possible to know the conductivity of solution, ohmic resistance ($R$) in ohm ($\Omega$) can be calculated from following formulations:

$$R = \frac{E}{l} \tag{2.26}$$

$$G = \frac{I}{E} = \frac{1}{R} \tag{2.27}$$

where $E$ is the potential in volt (V), $I$ is the current in ampere (A) and $G$ is the conductance in Siemens ($\Omega^{-1}$). Consequently, if it is possible to know electrical conductivity of solution, cell potential can be calculated from following equation:

$$E_{cell} = E_{cell}^{rev} + IR + \eta_a + \eta_c \tag{2.28}$$

where $\eta_a$ and $\eta_c$ are the anodic and cathodic overpotential, respectively.

## 2.3 Current and Distribution of Metal on Electrode Surface

Current distribution is another important factor that affects the thickness distribution on cathode surface, especially for structures having complex-shaped geometries. The shape of anode can also influence the current distribution. As shown in Figure 2.4, the deposited layer becomes thicker at the corners of the cathode resulting from non-uniform distributions of current. Anode-cathode distance also affects the distribution of metals on cathode surface since regions closer to the anodes have lower resistance to flow current which leads to higher current densities.

In order to obtain uniform distribution of metals on cathode surface some methods are applied such as fitting of appropriate shading parts on cathode surface to prevent the excess current, placing of anodes at different positions or using pulse current and pulse-reverse current techniques.

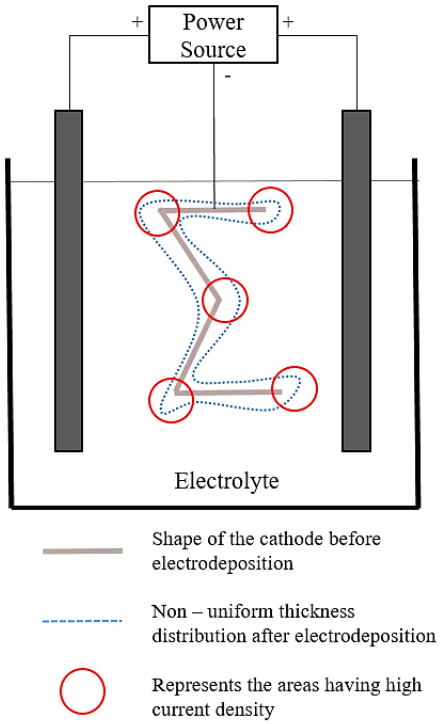


**Figure 2.4** Example of non-homogeneous thickness distributions and highest current density areas. Reproduced from [32].

## 2.4 Classification of Composite Materials

In order to achieve desired properties, composite materials are typically made by combining one or more material types in a weak matrix in particular forms and proportions under particular conditions [33]. Reinforcement materials and resin (Matrix) are the two constituents of composite materials. The kind of matrix being reinforced and the shape of the additional reinforcement element are used to categorize these materials [34]. Based on the shape of the reinforcement material, composite materials are divided into five types: Particle-Reinforced Composites: These are made by adding tiny granular filler materials to increase strength and rigidity. Materials known as particle composites are made by mixing one- or two-dimensional macroscopic particles with the matrix phase, or very tiny, microscopic particles that are believed to have zero dimensions. Macroscopic and microscropic particles have distinct effects on the composite material's behavior. The randomly distributed particle arrangement within the matrix resulting in anisotrophic properties is one factor

which distinguishes particle-reinforced composites from fiber and flake composites. Particle-based composites are very rigid and reasonably priced. Electrolytic composite coatings are frequently formed using these reinforcement forms. Composite coatings typically have a reinforcement volume ratio and particle sizes ranging from microns to even smaller particles placed in the matrix.

Polymer Matrix Composites (PMC): After the first contemporary synthetic plastics were developed in the early 1900s, the properties of plastic materials started to improve to the point where they could compete with other material types. Depending on the kind of reinforced matrix, composite materials are further categorized. Plastics' great surface quality, low density compared to metals, ease of shaping, and resistance to corrosion were major factors in their popularity. Efforts were made to reinforce plastic materials because of their comparatively low hardness and durability, despite their many superior qualities [35]. The most widely used polymer based composite material is GRP (Glass Fibre Reinforced Polyester/GRP, fibreglass), created in the late 1940s. GRP currently accounts for approximately 85% of all composite materials produced and is widely used in car bodies, sports vehicles, panels and boat hulls [36].Ceramic Matrix Composites (CMC): Ceramics are made by combining non-metallic elements such as carbon, nitrogen, oxygen, or boron with metallic or non-metallic elements. Ceramics are less dense and have lower electrical and thermal conductivity than metals, but they have significantly higher melting points, elastic moduli, hardness, and brittleness [37]. Carbon-Carbon Composites (CCC): Pure carbon particles, also known as the primary carbon component, are combined with carbon-ba to create carbon-carbon composites.

## 2.5 Composite Coatings Production Methods

The coating method to be employed is one of the main elements that influences the final composite coating's properties. Therefore, it is essential to have a thorough understanding of the chosen coating technique and the variables affecting it. Currently, thermal spraying, powder metallurgy, and electrochemistry are the three main methods commonly used in the production of composite coatings. In addition to these techniques, research indicates that some types of composite coatings (like those based

on nickel) are also made using laser cladding, hot isostatic pressing, and the combination of PVD and CVD methods [38]. Now, the electrochemical method is the most crucial procedure for composite coatings out of all of these [35]. In comparison to other coating techniques, the electrochemical method is more commonly used, especially in the production of metal matrix composite coatings, because of its benefits, which include low equipment requirements, high coating speed, and the creation of coatings with improved properties.

### 2.5.1 Thermal Spraying Method

The thermal spraying technique can be used to create a variety of composite coatings. Two distinct methods are used to carry out the spraying process: thermal spraying of High-Velocity Oxygen Fuel (HVOF) and plasma spraying. Composite coatings with excellent tribological qualities and corrosion resistance can be produced using this technique [35].

### 2.5.2 Powder Metallurgy Method

Powder metallurgy is one of the most employed techniques, particularly during the production of Metal Matrix Composites (MMCs). The two distinct manufacturing processes commonly employed in the powder metallurgy method for the production of MMC are solid and liquid processes. Although the liquid process is highly favored in metal matrix composite production because of being low-cost, it suffers from two major drawbacks [39]: Inhomogeneous dispersion by way of agglomeration or dendritic segregation of fibers or particles of ceramics inside the MMC structure. Melting points at interfaces lead to undesirable chemical reactions.

### 2.5.3 Electrochemical Method

Micro or nanoscale inert and hard particles are embedded into a coating bath using the electrochemical method, and particles are precipitated at the cathode as an alloy or metal matrix to form composite coatings [38]. This technique is relatively newer and has come along significantly since the 1970s in comparison to other coating technologies such as thermal spraying, plasma spraying, Physical Vapor Deposition (PVD), Chemical Vapor Deposition (CVD), and High-Velocity Oxygen Fuel (HVOF)

[38,40].Electroplating creates coatings with much superior mechanical and tribological properties at a lower cost than coatings created with powder metallurgy and high temperature pyrometallurgy [39, 41]. Different more advanced and better materials are currently produced thanks to the aqueous systems production method. The conventional properties of coatings electrochemically formed satisfy industrial needs, and such a process is supported by scientists in most instances in terms of advantages [42]. There are several worthwhile benefits compared to other composite coating procedures. These may be summarized as follows: It creates more uniformed coatings. A higher coating rate. The capability of working at low temperature. It is simpler to form complex shape surfaces. Electrochemical conditions for coating thickness and morphology regulation include temperature, pH, and current density.

A wide variety of particle and metal matrix pairs from aqueous suspensions may be used to create composite coatings of different types by using the electroplating process [41]. The electrochemical process has gained more attention during the last few years due to the greater emphasis on coating extremely small particles and the suitability of the electroplating process for this purpose [38]. Electrochemical composite coating is attained using two methods: Electroplating Deposition (EPD) and Electrophoretic Deposition (ELD). EPD process has been becoming increasingly popular in both academic and industrial processes due to its affordability and capacity to create high-performance coatings using current ceramic materials.The main benefits of this technique are its comparatively short coating time, the need for basic and affordable production equipment, the lack of significant limitations on the base material's shape, and the ease with which it can be altered for uses [43].

Colloidal particles suspended in an electrolyte migrate under the influence of an electric field (electrophoresis) in the EPD method, which is used to produce composite coatings. These particles are subsequently deposited on the electrode (cathode) surface along with the ions of the target material [44]. The charging of neutral particles with different coating solution additions is a defining characteristic of this process. These charged particles then move directly.

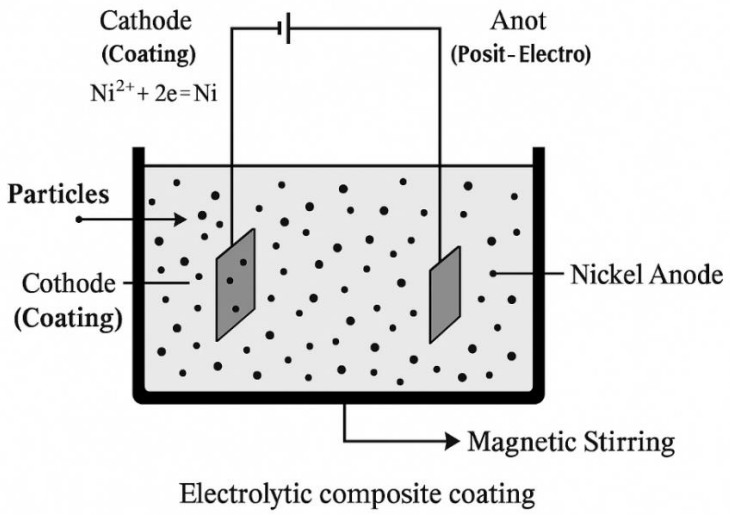


**Figure 2.5** Electrolysis system used in the production of electroplated composite coatings.

This is an experimental design technique in which two electrodes are placed in an electrolyte solution. A direct current (DC) power supply is used for the electrolytic coating process. The positive end of the power supply is connected to the electrodes called the anode and the negative end is connected to the cathode. This electrical connection initiates the electrochemical reactions that form the basis of the coating process, and the desired coating layer begins to form on the surface. When the system is passed through an electric current, the ions of the electrolyte are decreased on the cathode surface by the following reaction: $Me^{n++} + ne^{-} \rightarrow Me^{\circ}$ These electrons are provided to the reduction reaction by decomposition reaction of water or dissolution of the anode. As ions accumulate on the cathode surface through electrochemical processes, the accumulation of particles is usually due to mechanical adhesion, which is hydrodynamic condition dependent.

A wide variety of matrix and reinforcement materials can be used in the production of composite materials. There is a wide range of options for matrix materials in composite coatings. These include metals (e.g. Ni, Cu, Fe, Cr, Co, Ag, Au), alloys (e.g. NiCr, NiAg, steels, CuAg), polymers, ceramics (e.g. $Al_2O_3$, MgO x $ZrO_2$, BN, $Si_4$, Ti-Ge-C) and carbon. There is also a wide range of materials available in terms of reinforcement materials. These materials include; carbides (e.g. SiC, WC, TiC, $Cr_3C_2$), oxides (e.g.

$Al_2O_3$, $SiO_2$, $TiO_2$, $Cr_2O_3$), borides and nitrides (e.g. $Cr_3B_2$, $TiB_2$, TiN, AlN, BN), diamond, graphite, polymers, some metals (e.g. Cr, Al, W), glass and additives in the form of microencapsulated liquids. Selecting the appropriate reinforcement elements in this wide spectrum is very important in the production of composite coatings, since the properties of the matrix and the reinforcement must complement each other. The type and properties of the reinforcement to be distributed in the desired matrix (e.g. size, shape, concentration) are selected according to the targeted properties of the composite coating and the intended application area [45].

The following improvements can be observed in composite coatings [35]: Increased strength and binding efficiency, Improved tribological properties (e.g., increased wear resistance, decreased coefficient of friction, improved lubrication characteristics), Enhanced corrosion resistance, Increased thermal resistance, Improved catalytic properties, Reduced surface roughness and porosity, Enhanced decorative properties, Formation of barrier effects (e.g., thermal and electrical insulation).

Composite coatings exhibit much superior mechanical, tribological and corrosion properties compared to pure metal coatings. This improved performance, especially the advantages such as higher microhardness and wear resistance, can be largely explained by the dispersion hardening mechanism. According to this mechanism, three basic properties of the hardening particles added to the coating have a direct effect on the mechanical properties of the material: the hardness and size of the particles, the distribution pattern within the coating and their weight ratio in the coating structure [46].

Hard particles such as oxides, nitrides, borides and carbides evenly distributed within the coating significantly increase the resistance of the matrix material to deformation [46]. These hard and stable particles strengthen the structure by making it difficult for dislocations that cause deformation to move. At the same time, these particles prevent grain growth and provide a finer grain structure. Grain shrinkage is also a factor that directly increases the durability of the coating. In particular, the effect of this mechanism increases as the particle size decreases; therefore, particle size plays a critical role in dispersion hardening.

When microparticles are used during the coating process, they tend to accumulate only at the edges and boundaries of the crystals and are referred to as intracrystalline. In contrast, nanoparticles can be distributed both within the crystal and at its boundaries and are termed intracrystalline [42].

Another important parameter affecting the dispersion strengthening effect is the weight percentage of the particles within the coating. This value is directly influenced by the electrochemical parameters under which the coating process is carried out, such as temperature, pH, current density, electrolyte composition, and stirring rate [46]. As shown in numerous studies in the literature, increasing the weight percentage of reinforcing particles in the coating, reducing the grain size, and minimizing particle agglomeration all enhance the dispersion strengthening effect.

## 2.6 Parameters Affecting the Electrochemical Composite Coating Process

The process parameters used in the electrochemical coating method have a direct effect on the morphology, crystal structure, particle distribution, weight ratio and therefore all mechanical, tribological and electrocatalytic properties of the resulting composite coating. Therefore, researchers have been examining various process parameters both directly and indirectly for years in order to obtain composite coatings with certain properties.

They have shared their results in detail in the literature. In addition, a detailed understanding of these parameters contributes significantly to a clearer understanding of the particle deposition mechanism [46].

The basic parameters affecting the electrochemical deposition process of composite coatings are current density and type, operating temperature, pH level in the bath, bath content, stirring speed and zeta potential. These parameters are of critical importance in determining the microstructural properties and performance of the coating.

### 2.6.1 Current Type and Density

Two of the most important process variables in the electrochemical synthesis of

composite coatings are the type of current and the current density. They are also the most often researched parameters in composite coating research, according to the literature. Direct current (DC) and pulse current (PC), the latter applied at different frequencies (triangular, square, etc.), are the two current types commonly used in electrolysis.). When direct current is used to apply coatings, the current density stays constant during the entire process [46,47]. The phrase "current density" is used in electrolytic coating processes rather than just "current.". The amount of current flowing through a unit area is known as the current density, and it is commonly stated in $A/dm^2$ or $mA/cm^2$. It is unclear how current density affects the rate of particle incorporation. Fundamentally speaking, mass transfer controls the rate at which uncharged particles deposition occurs in the bath rather than the electric current. The particle/electrode interaction is regarded as independent of current density in this sense. On the other hand, increasing current density (up to the limiting current) improves the rate of metal deposition on the cathode surface. The quantity of particles integrated into the coating may be decreased by this faster rate of deposition. The particle/electrode interaction app is therefore applicable in such circumstances.

### 2.6.2 Working Temperature

The particle content of the final composite coating is greatly influenced by the plating bath's temperature. The temperature range appropriate for the metal plating bath being used is usually where the electrochemical composite coating process is carried out. A number of parameters that are impacted by temperature changes, including the particle surface composition, the electrolyte's density and viscosity, and the rate of metal deposition, are changed when the bath temperature is changed [46].

### 2.6.3 pH Value of the Plating Bath

Research has indicated that the particle content of composite coatings is significantly impacted by the pH level of the bath. Particle behavior shows that ions from the electrolyte, including $H^+$ ions, are adsorbed by particles added to the bath. Particle adsorption is thus greatly influenced by the pH of the bath, its composition, and the kind, form, and characteristics of the added particles. Electrophoretic mechanisms

can explain pH-related effects because of the formation of an ionic cloud around particles. Surface charges are carried by colloidal particles in aqueous solutions because of chemical binding, physical adsorption of ions from the bath, or ionization of surface groups. An ionic atmosphere typically surrounds these charged particles. For example, protons and $Ni^{2+}$ ions are adsorbed onto the surface of SiC particles in Ni/SiC composite coatings, giving them a positive charge and driving them to migrate toward the cathode under the influence of electrophoretic force. Another factor is particle size; larger particles have higher surface energy and can absorb more ions, which leads to larger ionic clouds. The electrophoretic velocity ($V_E$) of a spherical colloidal particle in an electric field (E) can be found using the Stokes model, which states that

$$V_E = \mu_E . E = q_p/(6\pi\zeta r) \tag{2.29}$$

Larger particles are therefore incorporated into the coating at higher rates due to their higher electrophoretic mobility [49,48]. Zeta potential is in addition to electrophoretic effects.

### 2.6.4 Bath Composition

The type of composite coating determines the content of the electrolyte bath to be used. Depending on the properties of the particles to be added, more flexibility can be provided in the composition of the bath. For example, Watts, sulfamate, high chloride, fully chloride or fluoroborate type baths can be preferred in nickel-based composite coatings. However, in order to obtain reliable metal deposition, the concentration of the base metal salts in the bath must be kept within certain electroplating limits.

Studies show that the bath content has significant effects on the particle deposition mechanism. For example, when $Al_2O_3$ particles of the same size and shape were added to different bath types, only nickel sulfate and copper cyanide baths were able to successfully form composite coatings containing $Al_2O_3$. In contrast, the same success was not achieved in chromium and copper sulfate baths. Additionally, studies have shown that the concentration of metal ions in the bath increases the amount of metal ion adsorption onto particle surfaces. Consequently, this improves particle

incorporation into the coating as well as particle-electrode interactions [46]. Surfactants such as saccharin, CTAB, and azobenzene derivatives (AZTAB) can also be added to the electrolyte. These cationic surfactants improve particle wettability and surface charge, which stabilizes suspensions. Electrostatic adsorption to the cathode surface is promoted by increased particle charge, improving both quanti and reducing agglomeration.

### 2.6.5 Stirring Rate

The liquid motion in the bath, the flow conditions created by mixing, directly affect the interaction of particles with the electrode and mass transfer. The main purpose of mixing in the composite coating process is to prevent particles from settling and clustering and to ensure that they are distributed homogeneously in the solution. Compared to pure metal coatings, this is much more important in composite coatings. Choosing the right mixing speed is of great importance at this point. If the mixing speed is too low, sufficient energy is not generated in the system and the particles clump together and settle. This causes fewer particles to be retained in the coating. On the other hand, when the mixing speed is too high, the particles hit the cathode surface violently and cannot remain there long enough; this again results in coatings with low particle content.

Also, the mixing speed depends on the particle size. For instance, SiC or $Al_2O_3$ nano-sized particles have a tendency to stick together because of their high surface energy. Consequently, higher mixing speeds are required to ensure that such particles are distributed evenly in the solution. However, if the speed is increased too much, particles attached to the cathode surface may be subjected to excessive forces and may break away from the surface. This may negatively affect the efficiency of the coating [50, 51].

### 2.6.6 Particle Influence

The intended qualities and market value of the composite coating are taken into consideration when choosing the particle material. The particle content in the finished coating is directly limited by elements like the concentration, size, and shape of the

particles in the bath. These qualities need to be considered in addition to selecting the appropriate particle type. Particle Concentration: The degree of particle concentration within a bath plays a pivotal role in shaping the particle content of the ensuing coating. However, it is oftentimes challenging to establish conclusive findings regarding its influence, given that it is dependent upon the attributes of the particles (including their type, size, and shape) and electrochemical factors such as pH, current density, and stirring speed [46]. As postulated by Guglielmi's "Two-Step Adsorption" model, an escalation in particle concentration augments the probability of particle adsorption on the cathode, thereby amplifying the weight percentage of particles within the coating. However, an excessive particle concentration gives rise to particle-particle interactions and agglomeration, thus diminishing incorporation a matter of significant concern in the context of baths containing nanoparticles [52]. Particle Size: The use of micro- and particularly nanoscale particles to improve and regulate the characteristics of composite coatings is becoming more and more popular as materials science advances. The electrochemical process and the properties of the finished coating are significantly influenced by particle size. Depending on the type of particle, different particle sizes have different effects on the coating's particle content. For instance, bigger particles in Ni/$V_2O_5$ coatings result in lower content, while larger particles in Ni-SiC composites increase the coating's SiC content while having no effect on Ni-$Al_2O_3$ [46]. Metal and alloy matrices have effectively incorporated nanoparticles with sizes ranging from 4 nm to 800 nm [52]. Achieving high particle loading and avoiding nanoparticle agglomeration in the bath are challenges [50]. Particle Shape: The impact of particle shape on electrochemical deposition is not well documented. The dopant particles in the bath can be of different shapes; fibrous, spherical, irregular or sheet shaped. Generally, fibrous particles are less incorporated into the coating due to their long structure. The shape of the particles is one of the most important factors determining the specific surface energy. This surface energy affects how much the ions will adhere to the particle surface and therefore the tendency of the particle to stick to the cathode surface [46].

### 2.6.7 Zeta Potential

Zeta potential is defined as the electrical potential that occurs at the interface of a solid

surface and the liquid in which it is located. Zeta potential is a function of the surface charge of a particle, the layers adsorbed at the interface (solid/liquid) and the composition of the solution in which the particles are suspended. The magnitude of the zeta potential possessed by the particles depends on the interaction of the particles in the electrolyte. Thus, the zeta potential value and the electrolyte in which the various particles are suspended allow us to predict the long-term stability of the particles [48]. If the particles have a large negative or positive zeta potential value, the particles will tend to repel each other. Therefore, the situation of the particles merging and clumping is eliminated. However, if the absolute value of the zeta potential value is low, there will be nothing to prevent the grains from approaching each other and agglomerating. The potential value that separates stable and unstable solutions is generally taken as +30 or -30 mV, accordingly stable solutions have a zeta potential more positive than +30 mV or more negative than -30 mV. There are three factors that affect the zeta potential. These are the pH value of the bath, the concentration of the additions and the ionic strength of the bath. The most important of these factors is pH. The pH increases with the addition of alkali into the solution. Thus, it causes the particle surface energy to become more negative or less positive. Since there will be a loss of OH- in the addition of acid, the surface becomes more positive. In this case, surfaces with more positive potential are formed at low pH and at high pH, surfaces with more negative potential are formed [49].

## 2.7 Particle Deposition Mechanism in Electrochemical Composite Coating Processes

### 2.7.1 Early Models

The mechanism of particle co-deposition with metals was first explained in the early 1960s because of growing interest in composite coatings. Whithers suggested that electrophoretic forces carry positively charged particles to the cathode. Williams and Martin described how particles added to the electrolyte are transported as a result of bath agitation and how the expanding metal layer mechanically traps them. Saifullin and Khalilova developed the first model to calculate the amount of particles incorporated into the coating, based on the principle of mechanical trapping. However,

Brandes and Goldthorpe argued that this approach ignores some fundamental elements particularly particle properties and electrolyte structure and that mechanical trapping alone is not a sufficient explanation. According to them, in order for particles to be incorporated into the metal layer, an electro-osmotic or similar attractive force must be effective that allows them to remain in a region close to the cathode surface for a sufficiently long time. The first attempts to explain particle retention in composite coatings can be summarized in two general steps: (1) particle transport towards the cathode and (2) interaction with the cathode surface [46].

### 2.7.2 Empirical Models

More thorough and eventually more realistic models were introduced after the initial developments. Guglielmi's 1972 model, which revolutionized our knowledge of particle incorporation mechanisms, was a significant turning point in this field. For the first time, both mathematical formulas and experimental data were used to explain the particle deposition process. In order to account for restricted physical conditions, similar models were later proposed with corrective parameters included.

#### *2.7.2.1 Guglielmi Model*

Based on the particle concentration in the bath and the applied current density, the Guglielmi model was created to quantitatively estimate the rate at which particles are incorporated into the metal coating. Particle properties and hydrodynamic conditions are disregarded in this model [52]. Furthermore, since it is hypothesized that high electrolyte concentrations serve as a shielding layer that stops particle charging, electrophoretic effects on the particles are not taken into account. The model states that there are two main steps in the deposition process. Particles physically approach the cathode in the first step, and because of their inherent motion, they are weakly adsorbed onto its surface. An ionic cloud envelops these weakly bound particles. The particles leave this ionic cloud in the second step and are firmly adsorbed onto the cathode surface [46]. According to this two-step model, a higher particle content in the final composite coating results from an increase in the concentration of particles in the electrolyte, which also increases the quantity of particles adsorbed on the cathode surface [53]. Taking into account the cathode's

effective surface area, the Langmuir adsorption isotherm provides a mathematical description of the first (weak adsorption) step.

$$\sigma = [(k\text{ø}) / (1 + k\text{ø})] \,.\, (1 - \theta) \tag{2.30}$$

The rate of strong adsorption (vp, particle incorporation rate) can be expressed as follows if cathodic polarization (ή) is considered in the second step.

$$vp = \sigma v_o e^{B\acute{\eta}} \tag{2.31}$$

In Equation 2.30, $v_o$ represents the rate constant, and B is the Tafel slope specific to the particle. The metal deposition rate is calculated according to Faraday's law:

$$v_m = (v_m J) / (nFq_m) \tag{2.32}$$

In metal deposition (considering the cathode surface area), for neutral particles, the term $(1 - \theta)$ is introduced, and according to the Tafel equation, the current density is dependent on the overpotential.

$$J = (1 - \theta) j_o e^{A\acute{\eta}} \tag{2.33}$$

If the volumetric fraction of particles incorporated into the metal coating is θ, and $\theta \ll 1$, the following expression is obtained:

$$\text{ø}/\alpha = [(M_m j_o^{B/A}) / (nFq_m v_o)] \,.\, j_o^{1-B/A} \,.\, (1/k + \text{ø}) \tag{2.33}$$

The parameters k, $v_o$, and B depend on the desired type of composite coating and must be determined experimentally using Equation 2.32. If a plot of ø/α' versus ø is drawn at constant current density, a straight line is obtained. From the intercept of this line at ø/α = 0, the value of 1/k can be calculated. According to Guglielmi's two-step adsorption model, an increase in particle concentration in the electrolyte leads to a greater amount of particles adsorbed onto the cathode surface. This, in turn, results in an increase in the particle content of the composite coating [53]. Guglielmi validated the applicability of his proposed model through experimental studies involving Ni/$TiO_2$ and Ni/SiC composite coatings. In these studies, when the experimentally determined k values were substituted into Equation 2.29, the result $\sigma \ll \theta$ was obtained,

indicating that the strong adsorption step is dominant.

Moreover, this model has been successfully applied to explain particle incorporation behavior in a wide variety of composite coatings, particularly those influenced by bath particle concentration and current density [46].

#### *2.7.2.2 Kariapper and Foster Model*

In the Guglielmi model, certain aspects regarding the role of the ionic cloud surrounding the particles remain unclear. One critical point is the behavior of particles that are weakly adsorbed onto the cathode surface while still enveloped by their ionic cloud. These particles must traverse their own ionic environment to firmly adhere to the cathode, which contradicts the assumptions represented by the "k" parameter in the Guglielmi equation.

In their proposed model, Kariapper and Foster emphasized the significance of particles that have various ions adsorbed from the electrolyte, and identified two important roles played by the adsorbed metal ions:

1. The positively charged metal ions induce electrostatic interaction between the negatively polarized cathode and the particles.

2. The metal ions, once adsorbed, are electrochemically reduced at the cathode, forming a physical barrier between the particle and the cathode surface.

In the model proposed by Kariapper and Foster, the following process parameters are used: q, E, J, L, a, b, N* and k**. Based on these parameters, and assuming k* is constant, the particle deposition rate in the Kariapper and Foster model is expressed by the following equation:

$$V_p = [N^* . k^* (qE + Lj^2 - ab) ø] / [(1 + k^*) (qE + Lj^2 - ab) ø] \quad (2.34)$$

The resulting equation has not been validated through experimental data; rather, it is a theoretical model that predicts potential peaks when a graph of particle content in the composite structure versus current density is plotted.

### *2.7.2.3 Buelens and Celis Model*

Celis et al. addressed the shortcomings of the Guglielmi model regarding the relationship between particle content in the composite and current density. By using their improved model, they were able to explain the appearance of specific peaks during the incorporation of $Al_2O_3$ particles into copper when operating at two distinct current density ranges.

At low current densities, the increase in particle deposition rate due to rising overpotential was found to be greater than the increase in the metal deposition rate. Under these conditions, $B < A$ (as presented in Equation 2.33), and the particle content in the composite ($\alpha$) increases with current density (j). In contrast, at higher current densities, $\alpha$ decreases with increasing j. In the transition region between these two regimes, the polarization curves for copper deposition start to deviate from the values predicted by the Tafel equation. This deviation is attributed to a shift in the control mechanism from charge transfer to concentration overpotential that governs the reduction of $Cu^{2+}$ ions [46].

Building on this approach, Buelens and his colleagues proposed a five-step mechanism for the formation of composite coatings. In the first step of the process, ions present in the bath adsorb onto the surface of suspended particles, forming an ionic cloud around each particle.As the bath is agitated, these particles are transported toward the hydrodynamic boundary layer. They then diffuse through the diffusion layer and reach the cathode surface. Finally, the particles, still surrounded by their ionic clouds, adsorb onto the cathode, and as some of the adsorbed ions are electrochemically reduced, the particles are incorporated into the metal matrix.

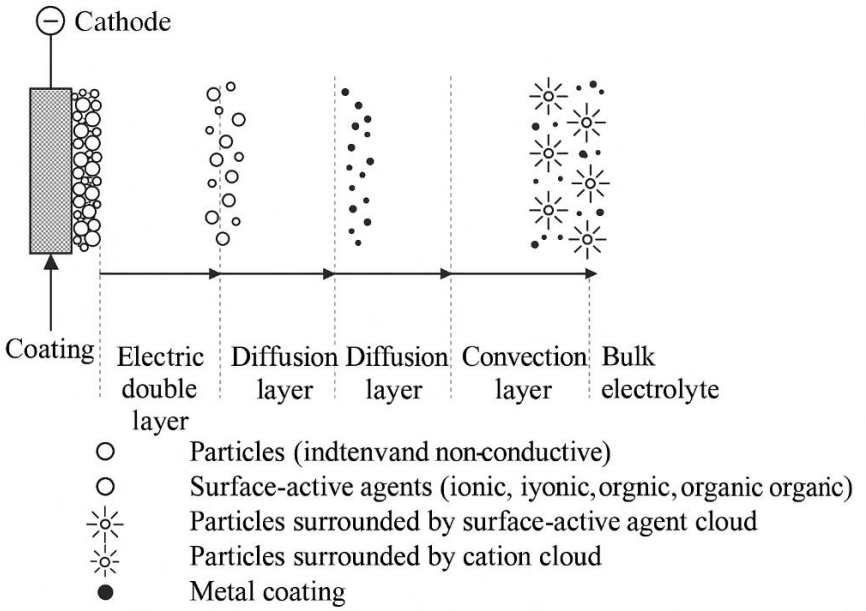


**Figure 2.6** Particle incorporation mechanism into metal coating according to the Buelens model [52].

The corresponding equation for this model is given below [54]:

$$\beta = (W_p N_p P) / [( M_m j)/ (nF) + (W_p N_p P)] \quad \textbf{(2.35)}$$

$W_p$ : Particle mass (Kg)

### *2.7.2.4 Hwang ve Hwang Modeli*

Hwang and Hwang developed an improved model by adapting and extending the models proposed by Guglielmi and Buelens et al. In this model, the particle deposition rate within three distinct current density ranges (low, medium, and high) is determined based on the electrode reactions involving particles that have various adsorbed ions. These reactions are governed by kinetic and/or diffusion-controlled parameters.

From the beginning of their experimental investigations on Co/SiC composite coatings, the primary focus was on $H^+$ reduction and the adsorption of $Co^{2+}$ ions onto the particle surfaces. The reduction of these ions at different current densities proceeds as follows:

- At low current densities, only the reduction of $H^+$ ions occurs.
- At medium current densities, the reduction of $H^+$ ions reaches its limiting rate, and $Co^{2+}$ reduction begins.

- At high current densities, the reduction rates of both ions reach their respective limiting values.

Similar to the Guglielmi model, the Hwang and Hwang model is expressed by Equation 2.36:

$$v_m = [M_m / (q_m nF)] \, . \, j_m(1-\theta) \tag{2.35}$$

The particle deposition rate has been derived separately for each of the three current density ranges. At low current density, the particle incorporation rate is determined by the reduction of adsorbed $H^+$ ions.

$$v_p = K_1 C^s_{H+} \sigma e^{B1n} \tag{2.36}$$

The term CsH represents the concentration of $H^+$ ions and decreases as a result of their reduction. At medium current density, the particle deposition rate consists of the sum of $Vp,H^+$, which corresponds to the limiting rate of $H^+$ reduction, and the metal ion reduction rate, which is similar to the $H^+$ reduction rate observed at low current density.

$$V_p = Vv_{p,H+} + K_2 (1- v_p/ v_{p,m}) C^b_m \sigma e^{B2n} \tag{2.37}$$

Finally, at high current density, the particle deposition rate is governed by diffusion, and becomes independent of both the current density and the concentration of adsorbed ions [46].

$$V_p = k_3 \sigma \tag{2.38}$$

## 2.7.3 Advanced Models

### *2.7.3.1 Valdes Model*

In 1987, Valdes developed a new model for composite coatings by working with a rotating disk electrode and considering the various transport mechanisms by which particles reach the cathode surface.

Based on the differential mass transfer equation, the particle concentration in the electrolyte, denoted as $C^*_p$, is expressed as follows:

$$dC^{*}_{p} / dt + dN_p / dx = 0 \quad (2.39)$$

The equation presented in Equation 2.39 consists of various mass transfer processes such as Brownian motion and convection. The convection term encompasses all forces and torques acting on the particle due to hydrodynamic migration, electromigration, and diffusion.

According to Valdes' electrode–particle–ion–electron transfer model, the particle deposition rate is expressed in the form of the Butler–Volmer equation.

$$V_p = K_o C^{s}_{iyon[} \exp [(-\alpha_T ήF)/(RT)]ή - \exp [((1-\alpha_T) ήF)/(RT)]ή] \quad (2.40)$$

By using this model, when a graph of the concentration of deposited particles in the solution versus current density is plotted, a distinct peak can be observed. Notably, this peak appears not at low current densities but rather near the limiting current density.

As a result, the Valdes model provides a much more comprehensive explanation of the particle transport mechanism compared to previous models. However, certain aspects regarding ion adsorption within the particle–electrode interaction remain open to discussion [46].

### *2.7.3.2 Guo et al. Model*

Guo et al. used quantities known as similitude numbers in their model to attempt to explain the mass transfer. The variables influencing the mass transfer determine the dimensionless values known as similitude numbers. The similitude number Shı is used to assess the particle coating rate if the absolute parameters, such as temperature, pH, and bath composition, are assumed to be constant.

$$Sh' = Co.Re^{c}.Dm^{d}.Sx^{e}.Gg^{f} \quad (2.41)$$

The constants in Equation 2.41 are determined using experimental data to refine and calibrate the model. The residence time of the particle on the cathode surface depends on the time it takes for a particle located in the bulk of the electrolyte to reach the cathode surface, which is governed by the flow velocity of the electrolyte [46].

### *2.7.3.3 Fransaer et al. Model*

Fransaer and associates. modified pre-existing theories of particle mass transfer and electrode-particle interactions for use in rotating disk electrode (RDE) composite coating research. By considering all of the forces and torques acting on the particle, this model was improved in several ways. These forces, which have a direct impact on the particle trajectory, include those resulting from fluid convection and particle motion. New equations describing particle trajectories were developed as a result of the existence of these forces. The limiting particle trajectory is calculated to find the net flux of particles toward the cathode surface. Trajectory theory, however, is invalid close to the electrode surface because it creates the false assumption of "Perfect Incorporation," which states that particle deposition never stops as current density rises. Rather, the model suggests an equation that calculates the likelihood of particle incorporation at the electrode surface based on the force balance acting on the particle.

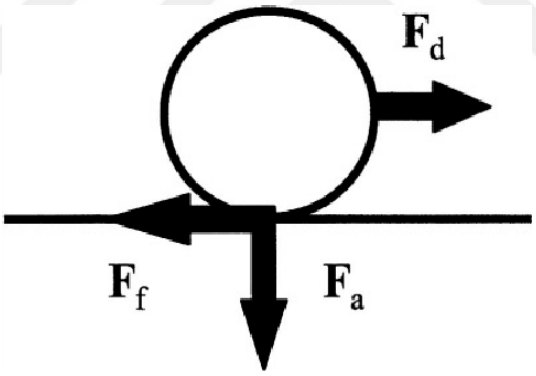


**Figure 2.7** Forces acting on a particle; Ff: frictional force, Fa: adhesion force, and Fd: detachment force attempting to remove the particle [46].

The particle's adhesion (Fa) to the cathode surface results in the frictional force (Ff). The opposing force that separates the particle from the cathode is denoted by (Fd). London–van der Waals forces, electro-osmotic forces, and electrophoretic forces are among the particle–electrode interaction forces that make up the adhesion force Fa. Nevertheless, this model is not supported by experimental data on adhesion force as a function of current density. Fa is also influenced by forces that are dependent on electrode geometry, such as hydrodynamic forces, lift forces, and gravitational forces.

Hydrodynamic conditions like electrode rotation are linked to the hydrodynamic force Fr. The particle deposition versus current density curve in this model shows no peak. According to experimental findings, a copper electrode which has a zero-electrode potential, and the highest electro-osmotic force is the ideal electrode for achieving maximum particle incorporation. In contrast to previous models, the trajectory-based model does not rely on many assumptions and is based on the generally acknowledged principles of particle mass transfer and particle–substrate interactions. The behavior of Zn/polystyrene and Ni/SiC composite coatings has been especially well-explained by this model in experiments [46].

### *2.7.3.4 Hovestad et al. Model*

The explanations of how surfactants affect particle incorporation through hydration force mechanisms have not been totally satisfactory, according to studies involving Zn/polystyrene composite coatings. According to Fransaer's theory, surfactants have a major impact on the mechanism of particle deposition because they are adsorbed onto the particle surfaces, changing their hydrophobicity and, as a result, the hydration force. It has been noted that the surfactants employed in Zn/polystyrene composite coating experiments significantly impact the deposited zinc's surface morphology and crystal structure.

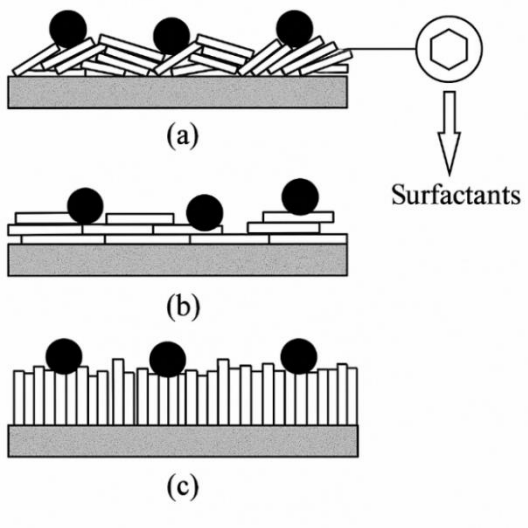


**Figure 2.8** Zinc coating growth morphologies: (a)irregular, (b) parallel, and (c) vertically hexagonal plates, where black represent coated particles [54].

Figure 2.8 provides a clear illustration of how particles are adsorbed onto the coating surface. Hovestad and associates. model shows that a particle's chances of being incorporated into a rough, indented surface are much higher than those of a smooth surface. This model predicts that coatings created on uneven surfaces will have a higher particle content [46]. Table 2.1 presents a comparative overview of key models that have significantly contributed to the literature in this field. While each model has its strengths in explaining specific behaviors, they also carry limitations in terms of assumptions or applicability. This summary provides a foundation for identifying the most relevant theoretical framework for interpreting the results of the present study.

**Table 2.1.** Comparison of Composite Coating Models

| Model | Basic Approach | Strengths | Weaknesses / Criticism |
|---|---|---|---|
| Guglielmi | Two-step adsorption (weak + strong) | First model with mathematical representation | Ignores hydrodynamics and electrophoretic effects |
| Kariapper & Foster | Electrostatic interaction + reduction of adsorbed metal ions | Emphasizes the role of adsorbed ions | The model is not experimentally validated |
| Buelens & Celis | Particle deposition related to current density and overvoltage | Explains two-region behavior via polarization | Verified only with $Cu/Al_2O_3$ systems |
| Hwang & Hwang | Reduction-based adsorption at three current density levels | Divides behavior into low, mid, and high current zones | Limited to $H^+$ and $Co^{2+}$ systems |
| Valdes | Mass transfer with convection, diffusion and migration effects | Integrates all transport mechanisms quantitatively | Still debated around adsorption mechanism |

**Table 2.1 (continued)** Comparison of Composite Coating Models

| | | | |
|---|---|---|---|
| Fransaer | Particle trajectory and force balance near cathode | Realistic, force-based explanation with RDE support | Complex and hard to generalize experimentally |
| Guo et al. | Dimensionless similitude numbers for transfer rate | Quantitative and scalable | Requires extensive calibration and constants |
| Hovestad et al. | Hydrophobicity and roughness impact through surface activation | Explains morphology–deposition relationship | Validated only for Zn/polystyrene coatings |

### 2.7.4 Ni-SiC Composite Coatings

One of the most popular and industrially favored coating types is electrolytic nickel (Ni) coating. As a result, Ni matrix composite coatings have drawn a lot of attention from researchers in recent years. Ni-based composite coatings have grown in popularity as a result of the electrochemical incorporation of different hard and insoluble particles (such as sulfate, high-chloride, all-chloride, fluoborate, and sulfamate) into traditional nickel baths to improve the properties of conventional Ni coatings. The market for advanced materials has seen a notable increase in demand for electrolytic Ni-based composite coatings reinforced with fine ceramic particles [41]. In comparison to many alloy or pure metal coatings, composite coatings with a nickel matrix created by dispersing various particles into electrolytic Ni coatings have demonstrated superior properties. These consist of resistance to oxidation, wear, corrosion, chemical inertness, microhardness, self-lubrication, and heat [55, 56]. In addition to these qualities, adding various solid particles can enhance magnetic and electrical properties [56]. To date, Ni has been successfully co-deposited with a wide range of particles, including carbon nanotubes, $AlO_3$, $SiO_3$, SiC, WC, $ZrO_2$, and $TiO_2$, as well as microcapsules containing liquids [55].

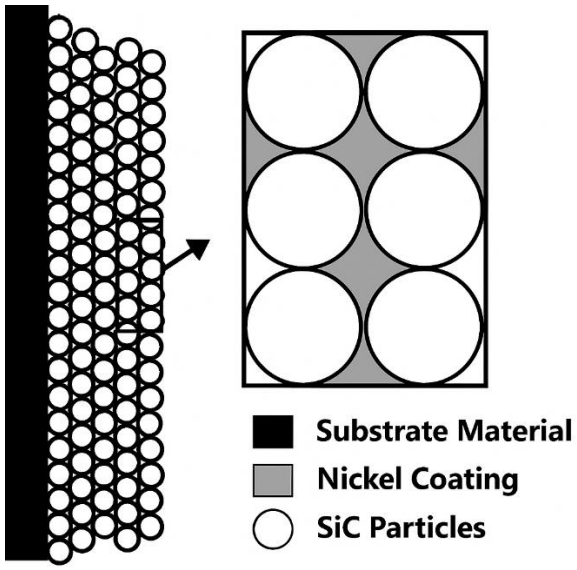


**Figure 2.9** Schematic Representation of a Ni/SiC Composite Coating [57]

Ni-SiC composite coatings were first developed in the 1960s by Grazon as a novel type of composite coating [41]. Since then, researchers have conducted extensive studies to optimize the co-deposition mechanism of nickel with SiC particles and to investigate the effects of various electrochemical parameters (such as current density, pH, electrolyte composition, stirring rate, and temperature) as well as SiC characteristics (including particle size, shape, distribution in the electrolyte, and concentration) on the resulting properties of Ni-SiC electrochemical composite coatings [48].In recent years, due to their enhanced mechanical and tribological properties, Ni-SiC composite coatings have found increasing applications, particularly in the automotive and aerospace industries [48]. In the automotive sector, these coatings are especially used on engine cylinders as a protective layer to reduce wear in car engines. Outside the automotive field, they are also applied to components exposed to high friction, such as bushings, rollers, nozzles, forming tools, and guiding elements, effectively extending the service life of machinery by protecting critical parts [55]. Apart from their excellent tribological performance, Ni-SiC electrochemical composite coatings exhibit superior corrosion resistance and higher catalytic activity against oxygen/hydrogen evolution reactions even in aggressive environments, compared to pure nickel coatings. The SiC particles, embedded within or between the nickel crystals (depending on their size), act as a barrier, thereby

hindering the corrosion pathways. In addition, due to their high thermal resistance, Ni-SiC coatings are successfully used in casting molds and high-temperature applications [53].

# CHAPTER 3

## EXPERIMENTAL PROCEDURE

Pre-treatment of the substrate was first done to guarantee surface activation and cleanliness before the coating process. After degreased with acetone, samples were etched in a weak acid solution. After surface preparation, boric acid, nickel sulfate, and nickel chloride were dissolved in distilled water to prepare the electrolyte solution for Ni-SiC composite electroplating. SiC particles were added into the bath with continuous stirring to ensure homogeneous suspension. The pH was brought to 4.5 with weakened sulfuric acid for electrodeposition, which was conducted at 50°C. During plating, a magnetic stirrer helped to keep SiC particles floating. To investigate how coating morphology and physical characteristics change, current density and deposition time were methodically changed. The coated samples were cleaned, dried, and set up for characterization after deposition. EDS was used to check whether the SiC particles were distributed in the coating and SEM to analyze surface and cross-sectional morphologies. Using a Vickers hardness tester, microhardness tests appropriated done, and with a pin-on-disc tribometer wear resistance was examined.

### 3.1 Preparation of Nickel-SiC Electrocomposite Bath

The electrocomposite coating bath in this experiment was made with a solution containing nickel ions, buffering agents to manage surface morphology, silicon carbide (SiC) particles, and supplemental substances. Literature information and initial tests helped us to optimize the solution of the bath. The main source of nickel ions in the bath, nickel sulfate ($NiSO_4 \cdot 6H_2O$), is vital in deciding surface integrity and coating thickness. $NiCl_2 \cdot 6H_2O$ (nickel chloride) raises the solution's conductivity which lets for more even distribution of current and supports anodic dissolution. pH buffer boric acid ($H_3BO_3$) keeps the pH constant and stops the development of rough coating surface structures. This encourages the coating matrix to better accept the particles. The ceramic reinforcing phase of SiC particles, which improve the coating's mechanical performance, are known for their great hardness and outstanding wear

resistance. To guarantee even distribution, all particles were preserved in suspension by constant magnetic agitation. Throughout the electrodeposition process, the bath was kept at 40-60 °C and the pH was set to 4.5 via diluted sulfuric acid.

**Table 3.1.** Composition of the Nickel-SiC Electrocomposite Coating Bath

| Chemical Compound | Function | Concentration (g/L) |
|---|---|---|
| Nickel Sulfate ($NiSO_4 \cdot 6H_2O$) | Source of nickel ions | 240 |
| Nickel Chloride ($NiCl_2 \cdot 6H_2O$) | Enhances conductivity, supports anode dissolution | 45 |
| Boric Acid ($H_3BO_3$) | pH buffer, improves coating smoothness | 30 |
| SiC Particles | Hard phase reinforcement, improves wear resistance | 20–40 |
| Distilled Water ($H_2O$) | Solvent / medium | ~1000 mL |

## 3.2 Base Material Selection And Sample Preparation

The good mechanical characteristics, corrosion resistance, and suitability for electrochemical coat applications of Aluminum 6061 alloy led it to be chosen as the material for the substrate in this research. A thorough surface pre-treatment was carried out to guarantee activation of the aluminum surface and elimination of toxins before the electroplating process started.

Pre-treatment started with soaking in an alkaline solution to clear away surface grease, organic debris, and any other contaminants. Samples were then washed with deionized water once more and subjected to acid activation, which broke down the aluminum surface's natural oxide layer and increased its reactivity. Following a second DI water rinse, the first zincate therapy was performed, when a thin layer of zinc was deposited over the aluminum surface to help grip and inhibit direct nickel deposition.

The first zinc layer was then erased in a specialized zincate stripping solution to rub the surface slightly and clean it. Following another rinsing with DI water, a second zincate treatment was given to create a more even and strong zinc layer. A last rinsing with DI water came next to clear all leftover compounds and ready the surface for the electroplating step. The sequential pre-treatment steps described above are illustrated

in Figure 3.1.

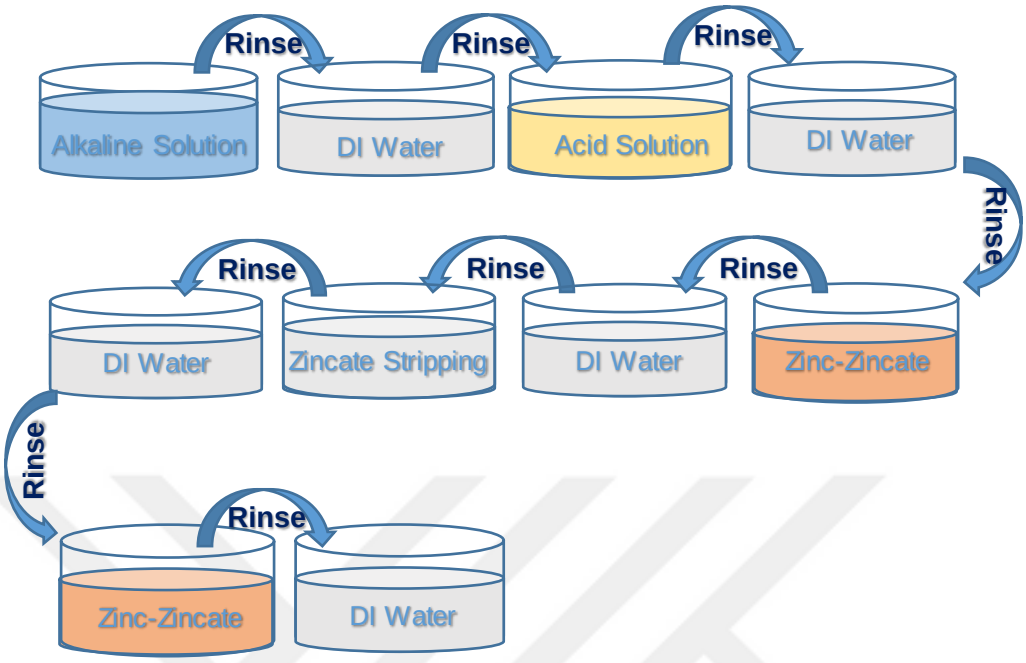


**Figure 3.1** Pre-treatment steps for aluminum substrate.

## 3.3 Nickel-SiC Electrocomposite Coating Study

Electrolytic coating of Ni/SiC composite coatings was carried out in typical semibright baths. The main components and concentrations of the bath used in all experimental series were: 250 g/L $NiSO_4 \cdot 6H_2O$, 40 g/L $NiCl_2 \cdot 6H_2O$ and 40 g/L $H_3BO_3$. The bath was prepared freshly in a volume of 1000 mL with analytical grade chemicals and distilled water. The concentration of the main bath components was kept constant in each coating process, pH, current density, bath temperature and SiC amount were changed.

The experimental setup for the coating processes was carried out by electrolytic method using a direct current source. Al6061-T6 plate with a surface area of 5.5 $cm^2$ was used as the cathode material. Pure nickel was preferred as the anode and placed in a titanium anode basket. In the experiments, the coating processes were carried out by precisely controlling the current and temperature parameters. The general view of the experimental setup used is presented in Figure 3.2.

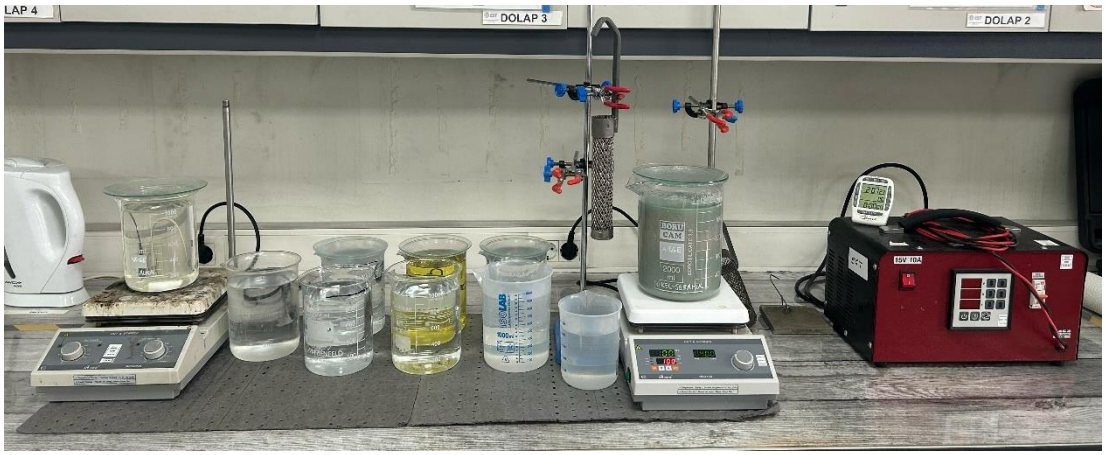


**Figure 3.2** Experimental setup where the coating processes were carried out.

In the experiments, a specially designed rectifier with a 15 V, 10 A capacity served as the direct current source. An MTOPS MS300 HS model heated magnetic stirrer was utilized to control the temperature and guarantee the homogeneity of the solution in the coating bath. A digital temperature indicator aided in the measurement and regulation of solution temperatures. A WTW ProfiLine pH 3110 portable pH meter was used to measure the coating solution's pH value, and the appropriate corrections were made. Throughout the coating period, temperature, pH, and current levels were regularly checked. The electrolyte temperature was maintained throughout the coating procedure, and the solution was thoroughly mixed. To get rid of any loose particles on the surface, the samples were cleaned before coating and rinsed with pure water after. Coating procedures were conducted under control and repeatable conditions using the experimental setup that was created in this manner.

### 3.3.1 Ni-SiC Composite Coating Experiments

Ni-SiC composite coatings were formed on Al6061-T6 plate and EN AC 48000 casting sample surfaces under different concentrations of SiC particles and coating parameters. The experiments were carried out at three different pH levels (3.5, 4.0 and 4.5), and the temperature, SiC concentration, current density and coating time parameters were changed for each pH value. The parameters used in these experiments were determined as follows:

**Table 3.2.** Parameters and Levels for Ni/SiC Composite Coating Experiments

| Parameter | Exp 1 | Exp 2 | Exp 3 |
|---|---|---|---|
| Temperature (°C) | 45, 55, 60 | 45, 55, 60 | 45, 55, 60 |
| SiC Concentration (g/L) | 20, 30, 40 | 20, 30, 40 | 20, 30, 40 |
| Current Density ($A/dm^2$) | 2.5, 5, 10 | 2.5, 5, 10 | 2.5, 5, 10 |
| Coating Time (min) | 60, 75, 90 | 60, 75, 90 | 60, 75, 90 |
| pH Value | 3.5 | 4.0 | 4.5 |

As a result of preliminary experiments and literature comparisons on three different pH values (3.5, 4.0 and 4.5) used in this study, it was seen that the desired surface quality, coating thickness and mechanical properties could be achieved only under pH4.0 conditions. In coatings performed at pH 3.5, visible homogeneity problems and distribution disorders were detected on the surface. In particular, the irregular accumulation of SiC particles on the surface caused unwanted porosity and matting in the coating. Therefore, this parameter group was eliminated from the study. In pH 4.5 conditions, it was determined that the coating integrity was low, adhesion problems and a structure prone to cracking occurred under the surface. Therefore, the pH 4.5 group was also excluded from the evaluation. In light of all these findings, pH 4.0 value was chosen as the focus of the study as it gave the most stable and reproducible results under the parameters of coating time, temperature, current density and SiC concentration.

## 3.4 Characterization Studyies

### 3.4.1 X-Ray Diffraction (XRD) Analysis

X-ray diffraction was used to examine the phase analysis structures of the resulting coatings (Bruker D8 Advance, Figure 3.3). Using Cu-Kα as a monochromatic X-ray radiation source, all studies were conducted at 30 kV, 15 mA, 5–85° , and a fixed scanning speed of 5 degrees $min^{-1}$. To avoid diffraction peaks from the base material, the X-ray material entrance angle was maintained at 2°. By comparing the acquired X-Ray diagrams with the standard data in the JCPDS (Joint Committee on Powder

Diffraction Standards) data file, the phase structures of the coatings were ascertained.




**Figure 3.3** D8 Advance XRD device.

### 3.4.2 Hardness Measurements

Fischer HP100 X-Y PROG (Figure 3.4) type ultra-microhardness instrument was used to measure the coatings' hardness values. A force that could penetrate up to 1/10 of the indenter's coating thickness was chosen in order to prevent the base material's influence on the hardness tests. Accordingly, hardness values were taken from 25 distinct sites for each sample, 60 steps were taken with a 1 second pause between steps, and 30 mN of force was applied to do the measurements. Before taking a microhardness measurement, the sample was examined under a microscope, and 25 locations were chosen to test the hardness.



**Figure 3.4** Fischer HP100 X-Y PROG brand ultra microhardness device

The hardness values were then obtained by moving the table the sample was put on under the microscope's indenter. For every hardness measurement, indentation depth-load curves were acquired at the conclusion of the test. The average hardness value of the coatings was determined using the arithmetic average of the remaining values after excluding curves that had substantial deviations from the average values in either the positive or negative direction and data that deviated significantly from linear behavior.

### 3.4.3 CSM-Tribometer

Using the CSM-Tribometer (Figure 3.5) instrument, reciprocating wear tests (Reciprocating) were performed against $Al_2O_3$ balls (ø10 mm) in an oil-free environment at 26 ± 2 temperature and 48 ± 5% relative humidity. The coatings underwent wear tests with a constant linear wear rate of 2 cm s-1, a frequency of 10 Hz, and a force of 2 N. During the studies, the $Al_2O_3$ wear ball traveled 50 meters, and its ½ amplitude value was 2.35 mm. Figure 3.5 shows the brand of wear equipment used in reciprocating wear tests. During wear testing, inert ball $Al_2O_3$ is used to reduce tribochemical reactions and guarantee that the coating-ball system's friction characteristics are more precisely identified. It is simpler to compare the coatings in this instance.

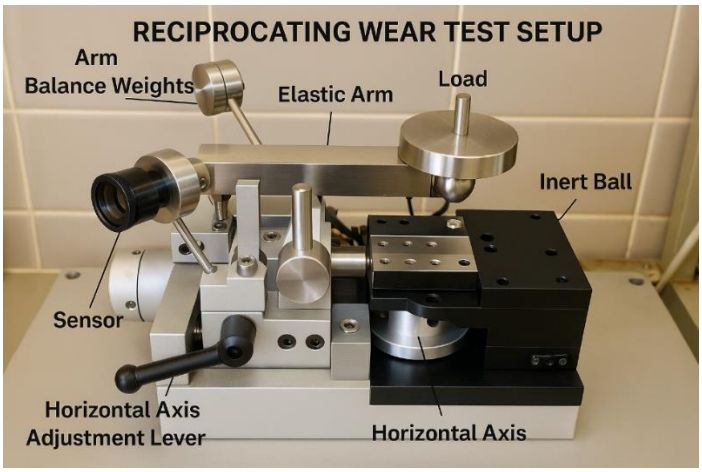


**Figure 3.5** CSM Tribometer brand wear device assembly

In the wear testing, the cleanliness of the $Al_2O_3$ ball and sample is crucial. The ball and sample were ultrasonically cleaned with alcohol for ten minutes before to each experiment since any dirt or oils that may be present on these parts will significantly alter the friction coefficient values that need to be determined.

### 3.4.4 SEM-EDS Analyses

Cross-sectional structures of the produced Ni-SiC composite coatings were examined by scanning electron microscopy. JEOL JSM 6060LV scanning electron microscopes were used in the microstructure examination of the coatings. The presence of SiC in the coating structure and its wt.% ratio was determined by EDS analysis.



**Figure 3.6** JEOL JSM-6060LV Scanning Electron Microscope used for cross-sectional characterization of Ni-SiC composite coatings.

# CHAPTER 4

## RESULTS AND DISCUSSION

### 4.1 Effect of Deposition Time and Temperature on Coating Thickness

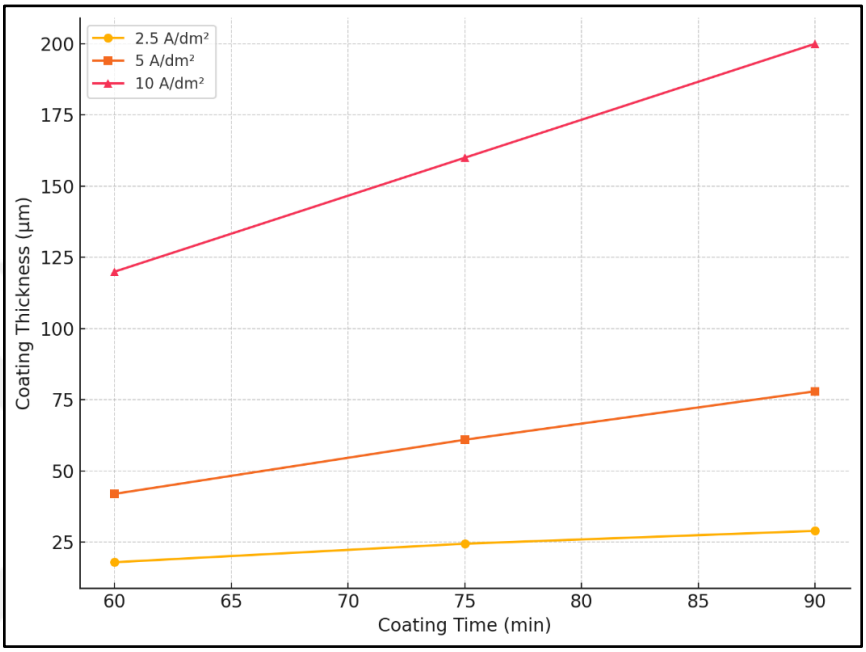


**Figure 4.1** Variation of coating thickness (µm) as a function of coating time (min) for different current densities (2.5, 5, and 10 A/dm²) under constant temperature (55 °C) and pH 4.0 and 0,40 /L SiC

Variation of coating thickness with time of deposition was presented in Figure 4.1, for three different current densities, 2.5, 5, and 10 A/dm² for the same electrochemical conditions, pH 4.0 and 55°C. Naturally, the thickness of the coating increases with deposition time and current density. At any current density, the longer the deposition time, the thicker the deposit owing to the prolonged transfer of charge. At 75 min, the coating thickness is about 24.5 µm at 2.5 A/dm², 61 µm at 5 A/dm² and 160 µm at 10 A/dm². This behavior is preserved at all time scales, indicating that the current density is a crucial factor in controlling the growth rate of the deposited layer. Increased current densities results in faster deposition due increased flux of metal ions on the substrate.

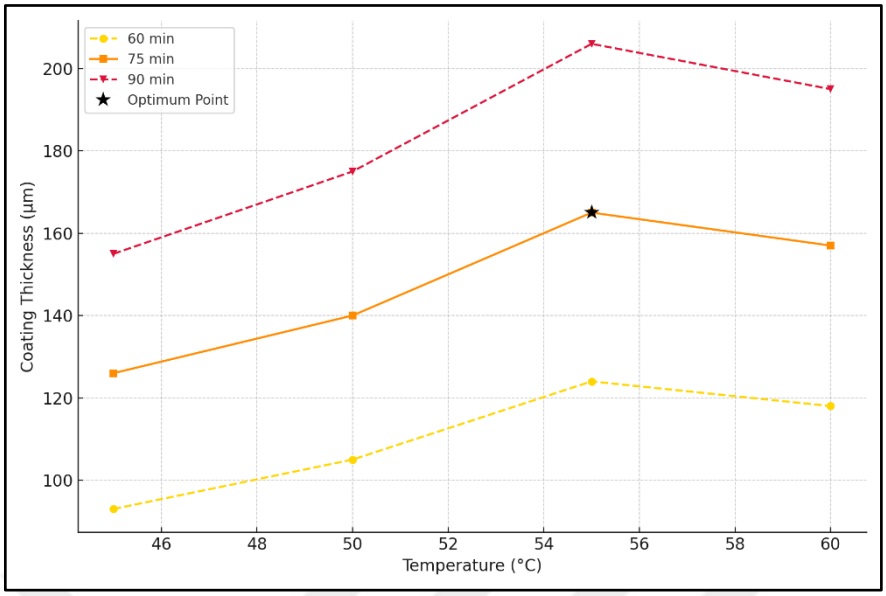


**Figure 4.2** Variation of coating thickness (µm) as a function of bath temperature (°C) for different deposition times (60, 75, and 90 minutes) at constant current density (10 A/dm²) and pH 4.0 and 0,40 g/L SiC

Figure 4. 2 reports the influence of bath temperature on the coating thickness for three deposition times (60, 75 and 90 min) in fixed electrochemical conditions (pH 4.0, 10 A/dm²). At all times, the coating thickness increases monotonously with increasing temperature from 45 °C to 55 °C, due to enhanced ionic conductivity and deposition kinetics. Always, the maximum value of thickness is situated at 55°C, with a value of 165µm at 75 min. Beyond this temperature, a slight drop is noted at 60°C is more pronounced at 90 min of deposition. This might be caused by fast side reactions or thermal instability of the bath in such a way that allows no layer to develop properly. This trend indicates that 55 °C is the best temperature, which provides a ductile and high thickness, for the coating.

## 4.2 Microstructural Analysis of Ni–SiC Coatings

In this section, the microstructural and compositional properties of Ni–SiC composite coatings obtained under different current densities were investigated in detail. The data obtained were evaluated on samples carried out, especially under pH = 4 and SiC = 40 g/L conditions; the results obtained under these conditions were determined as the most efficient parameter range in terms of coating quality and SiC particle adhesion.

In the examinations, coating thickness, homogeneity and structural integrity were analyzed with SEM images; and especially the SiC amount was quantitatively evaluated with EDS results. Samples with a SiC ratio between 7–13% were accepted as successful and in this context, only samples close to optimum (Sample A-A1-B-B1-C-C1) were discussed in detail. The effect of different current densities (2.5, 5 and 10 A/dm²) on coating morphology and particle integration was evaluated comparatively and the results were interpreted by relating them to the literature.

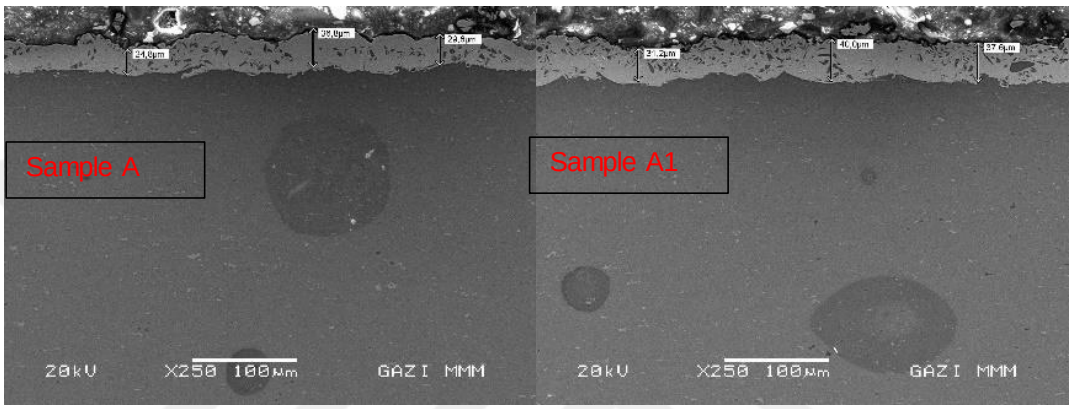


**Figure 4.3** Same sample A and A1 both coated under 4 pH 55 °C 75 min 0,40g/L SiC 2.5 A/dm² current density.

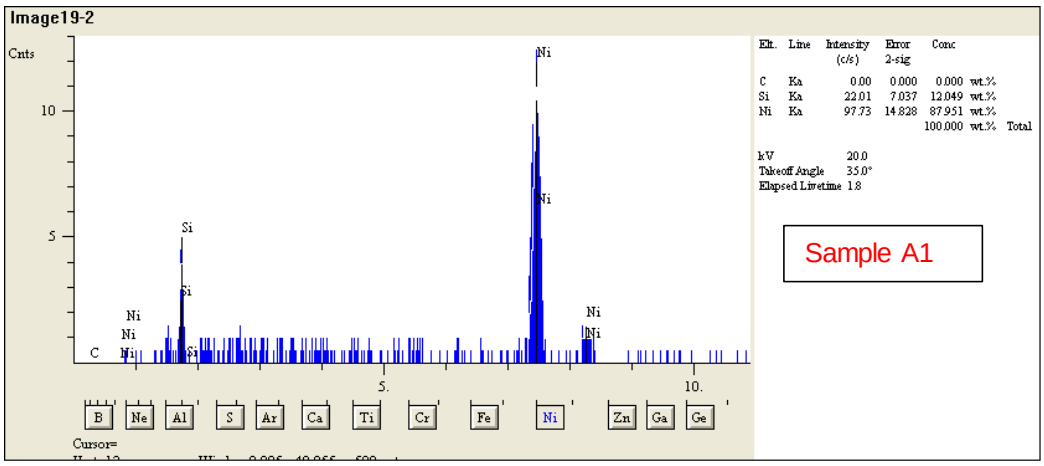


**Figure 4.4** EDS spectra of Sample A (top) and Sample A1 (bottom), revealing the elemental composition of the Ni–SiC coatings.

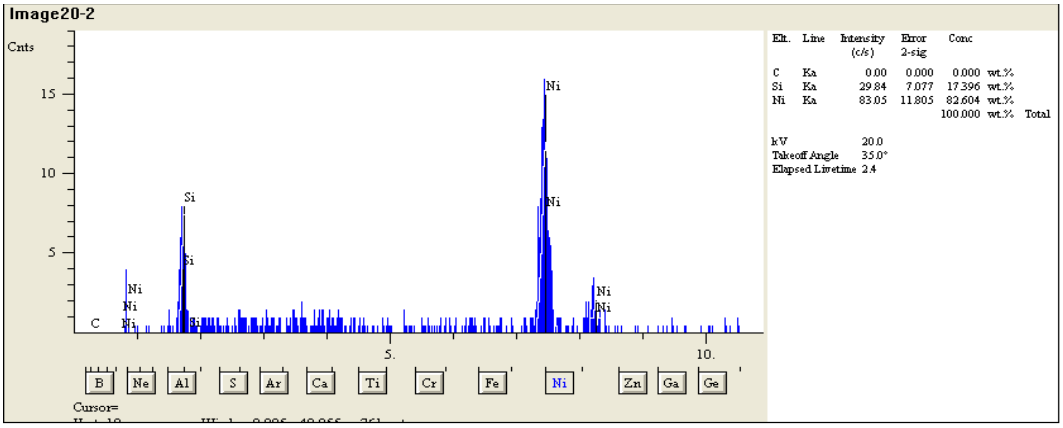


**Figure 4.4 (continued)** EDS spectra of Sample A (top) and Sample A1 (bottom), revealing the elemental composition of the Ni–SiC coatings.

When samples A and A1 were coated at a low current density of 2.5 A/ dm², significant limitations were observed in their coating thickness and SiC incorporation efficiency. The relatively thin layers (~22–27 μm) with internal void-like regions and obvious inhomogeneities in the SEM cross-sections suggest poor structural integrity. Low silicon contents of 2.63 weight percent (Sample A) and 3.10 weight percent Sample A1 were confirmed by EDS analysis; these values are significantly below the ideal SiC range of 7–12 weight percent.

These results are consistent with those of Celis et al. (2000) [58], who discovered that electrochemical reactions that efficiently co-deposit non-metallic particles like SiC cannot be driven by low current densities. Similarly, Benea and Dorneanu (2007) [59] demonstrated that SiC incorporation efficiency increases with current density due to enhanced convective transport and surface entrapment. Low current density results in uneven coatings, inadequate SiC impregnation, and insufficient mechanical reinforcement potential. These samples serve as a baseline for comparing improvements at higher current conditions.

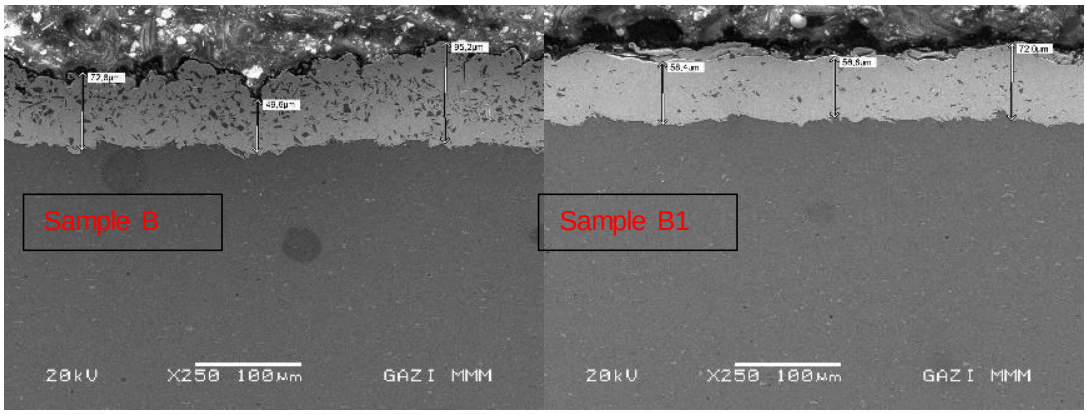


**Figure 4.5** Same sample B and B1 both coated under 4 pH 55 °C 75 min 0,40g/L SiC 5 A/dm² current density.

The microstructure and chemical composition results of the B and B1 samples coated at 5 A/dm² current density are evaluated. When compared to the previous 2.5 A/dm² group, a significant increase in the coating thickness was observed in both samples. According to the SEM images, the thickness of the B sample was measured between 49–73 µm, and the thickness of the B1 sample was measured between 55–72 µm Figure 4.5.

Although the increase in the coating thickness in these samples is a favorable development, the distribution of the SiC particles within the coating is not as homogeneous as expected. Especially in the B sample, it was observed that the SiC particles were clustered within the coating, concentrated in some areas, but almost absent in some areas. Although the B1 sample seems to have a more uniform structure, when examined in detail, it is noticed that the particles are not distributed homogeneously here, but are collected in certain areas.

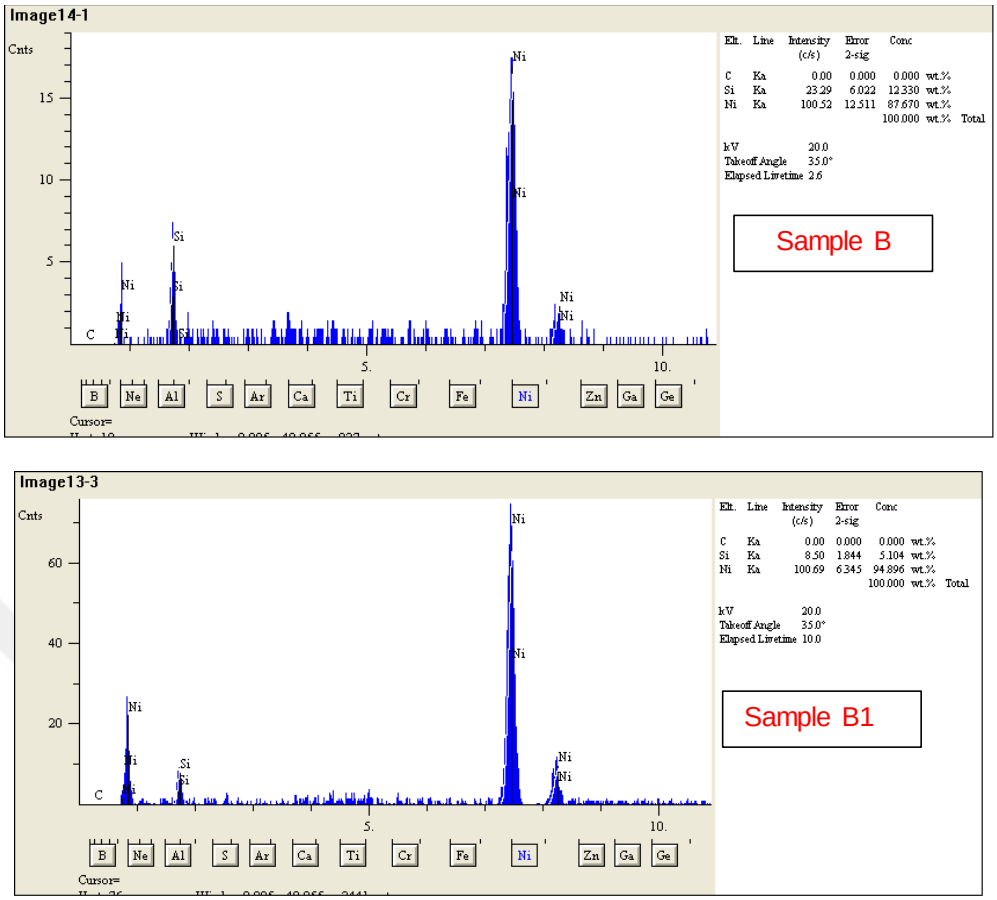


**Figure 4.6** EDS spectra of Sample B (top) and Sample B1 (bottom), revealing the elemental composition of the Ni–SiC coatings.

These observations are also supported by the EDS analysis results Figure 4.6. The 23.29% Si content detected in sample B is above the ideal range of 7–12%. The 8.50% Si content in sample B1 is in this range. However, it was observed that the particles were not distributed evenly in sample B1.

These findings also support the studies in the literature. According to the model proposed by Guglielmi (1972), during the coating process, the particles first adsorb on the surface and then become physically trapped in the growing metal matrix. The efficiency of this second step is directly dependent not only on the applied current density but also on parameters such as the mixing dynamics in the bath, the surface charge of the SiC particles and the suspension stability. Chandrasekar and Pushpavanam (2008) stated that in cases of low dispersion stability, the particles settle irregularly in the coating [60,61].

As a result, these two coating samples performed at a current density of 5 A/dm² provide positive results in terms of thickness, but they have some problems such as the SiC particles not being distributed homogeneously in the coating and the content amount increasing uncontrolledly. This situation shows that not only the current density but also the physical conditions in the bath should be optimized in detail.

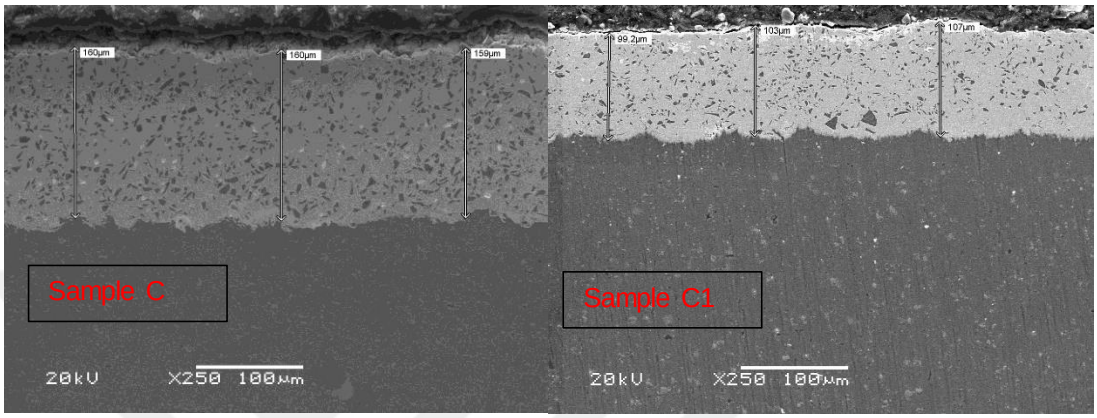


**Figure 4.7** Same sample C and C1 both coated under 4 pH 55 °C 75 min 0,40g/L SiC 10 A/dm² current density.

Figure 4.7 presents the cross-sectional SEM micrographs of Sample C and Sample C1 coated under a current density of 10 A/dm². It is observed that the coatings obtained at this high current level are denser, more continuous and the SiC particles are embedded more homogeneously in the structure compared to the coatings made at 2.5 and 5 A/dm². In particular, the fact that the SiC particles are evenly distributed in the nickel matrix shows that particle transport and surface adhesion in the bath are more effective at this current density.

Compared to low current densities, lower porosity and more consistent layer thickness were obtained throughout the coating thickness in Sample C and C1 samples. The clear and sharp transition between the coating and the substrate surface also reveals that a strong adhesion is formed thanks to the compact structure formed.

All these findings show that a current density of 10 A/dm² provides both homogeneous reinforcement distribution in terms of mechanical strength and increases microstructure integrity in Ni–SiC composite coatings. Therefore, considering the

limited particle retention observed at lower current densities, it can be said that 10 A/dm² is much more advantageous.

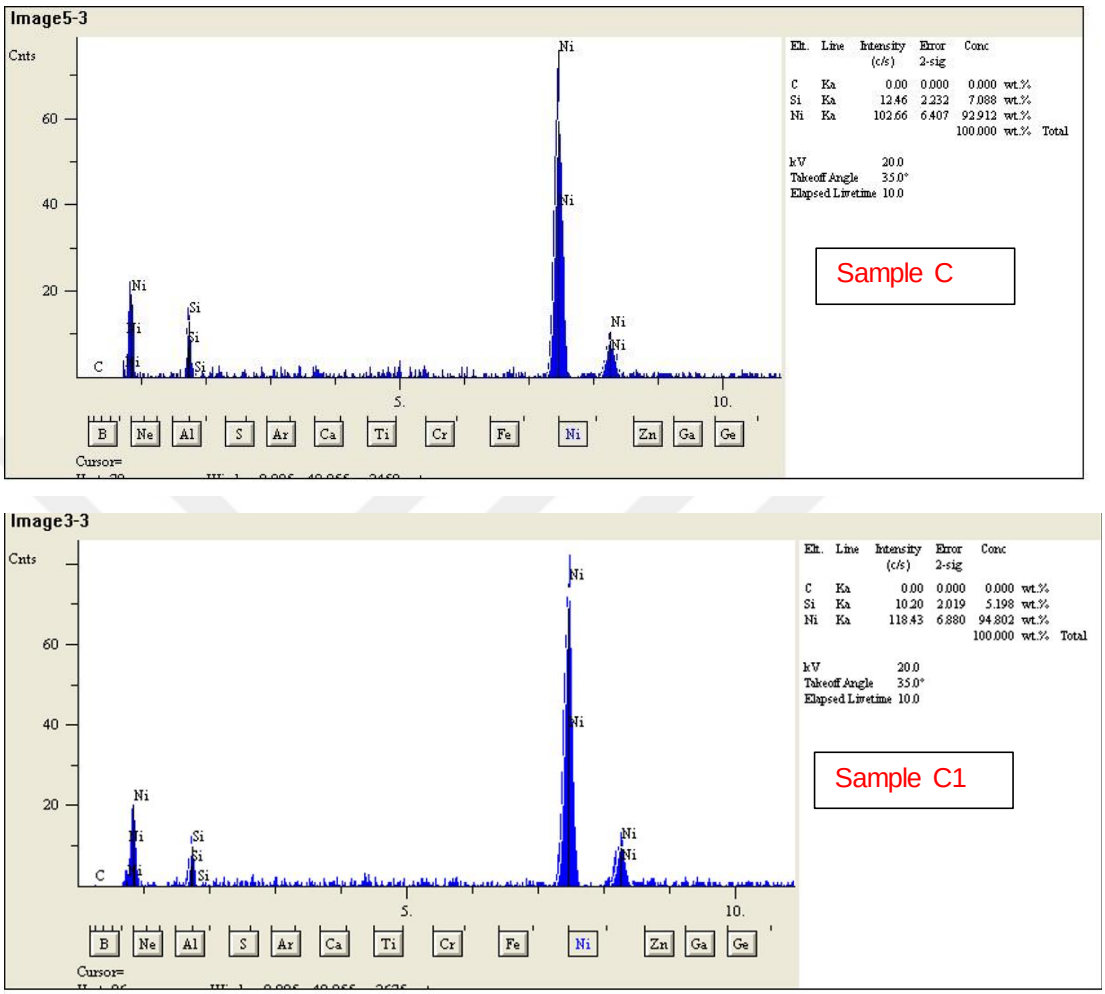


**Figure 4.8** EDS spectra of Sample C (top) and Sample C1 (bottom), revealing the elemental composition of the Ni–SiC coatings.

EDS spectra of Sample C (top) and Sample C1 (bottom) are given in Figure 4.8. The elemental composition of the Ni–SiC composite coating was successfully analyzed in both samples. According to the analysis results, 12.46% silicon was detected in Sample C and 10.20% in Sample C1. These values are within the 5–14% range accepted for effective reinforcement effect in the literature and show that SiC particles were successfully embedded in the coating structure. The higher Si content in Sample C may mean that the suspension in the bath is more stable or that the parameters during coating (such as mixing, temperature, current density) support particle transport more

effectively. However, sufficient Si was also obtained in Sample C1, indicating that a homogeneous reinforcement structure was formed. The absence of a carbon peak in both spectra reveals that the surface is clean and free from organic residues. The apparent intensity of nickel (Ni) signals indicates that the nickel matrix has been successfully precipitated, and the coating has a strong structure in terms of metal phase. As a result, these analyses show that a current density of 10 A/dm² is effective in effectively integrating SiC particles into the structure. However, it is clear that not only current density but also parameters such as bath stability, suspension efficiency and mixing are decisive in coating quality.

## 4.3 Influence of SiC Concentration and Current Density

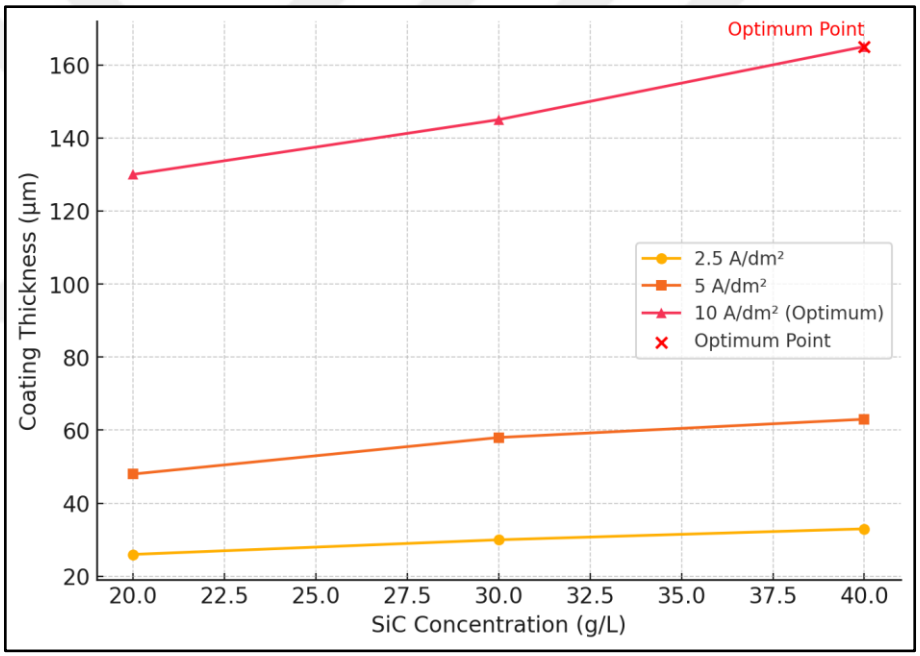


**Figure 4.9** Effect of SiC concentration on coating thickness at different current densities

In Figure 4.9, the effect of SiC concentration on the coating thickness is presented comparatively using different current densities in experiments carried out under a fixed coating time of 75 minutes. At all current levels, an increase in coating thickness was observed with the increase in SiC concentration. This situation can be explained by the integration of more SiC particles into the metal matrix with the increase in the amount of particles in the bath.

However, this increase varies depending on the current density. While the coating thickness increased limitedly at low current density (2.5 A/dm²), the coating thickness reached approximately 165µm at a current density of 10 A/dm², especially at a SiC concentration of 40 g/L. This value was evaluated as the highest thickness within the scope of the study when the fixed time of 75 minutes was taken into account and these conditions were determined as the optimum parameter set.

At high current density, the increase in the amount of ions and particles transported to the electrode surface increases the deposition rate and therefore the thickness. This shows that the coating thickness is directly related not only to the amount of SiC but also to the electrokinetic conditions. This study showed that for a coating time of 75 minutes, the most efficient result was obtained with a current density of 10 A/dm² and a SiC concentration of 40 g/L.

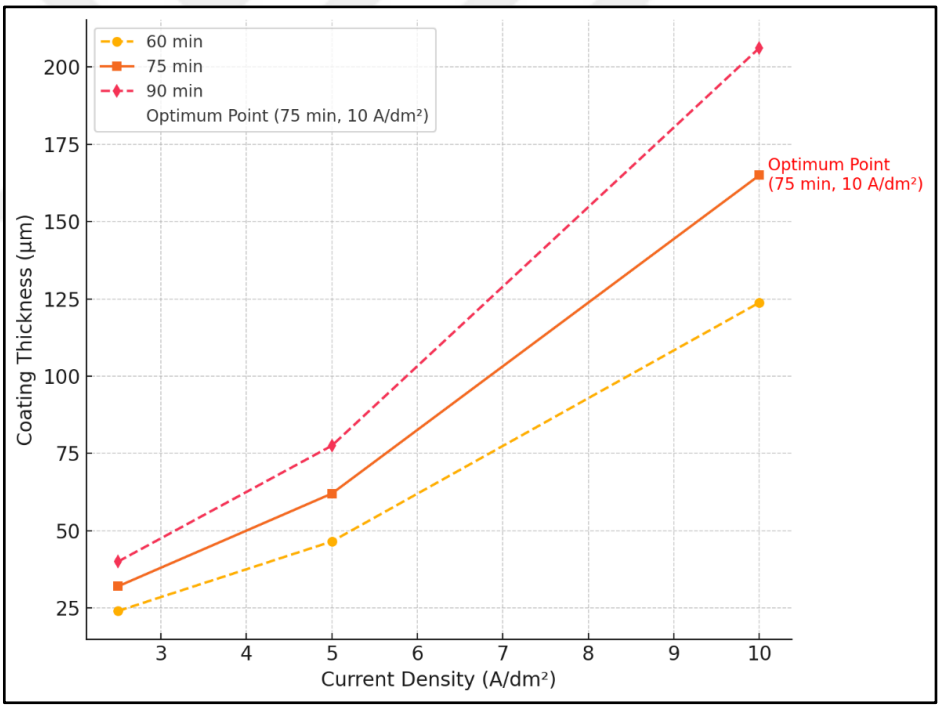


**Figure 4.10** Variation of coating thickness (µm) as a function of current density (A/dm²) for different deposition times (60, 75, and 90 minutes). Bath temperature and SiC particle concentration were fixed at 55 °C and 40 g/L, respectively.

As seen in Figure 4.10, increasing the current density had a direct effect on the coating thickness. Experimental data show that increasing the current density from 2.5 A/dm²-

5A/dm² to 10 A/dm² increased the coating thickness from 31 µm at 2.5 A/dm², to 62 µm at 5 A/dm², and reached 165 µm at 10 A/dm². The primary cause of this increase is the acceleration of deposition caused by more metal ions being drawn to the electrode surface at high current densities. Thus, more metal layers are formed per unit time, which causes the coating thickness to increase. In this context, in this study, 10 A/dm² current density was evaluated as the optimum point considering the maximum thickness value obtained and the coating quality.

This trend is an expected result in terms of the electrodeposition process. As time increases, the amount of metal ions deposited on the electrode increases and a thicker coating layer is formed. However, it should not be forgotten that this increase may increase surface roughness in the future or make it difficult for SiC particles to be distributed homogeneously. Therefore, when determining the coating time, not only the thickness but also the surface quality and functional performance should be taken into consideration.

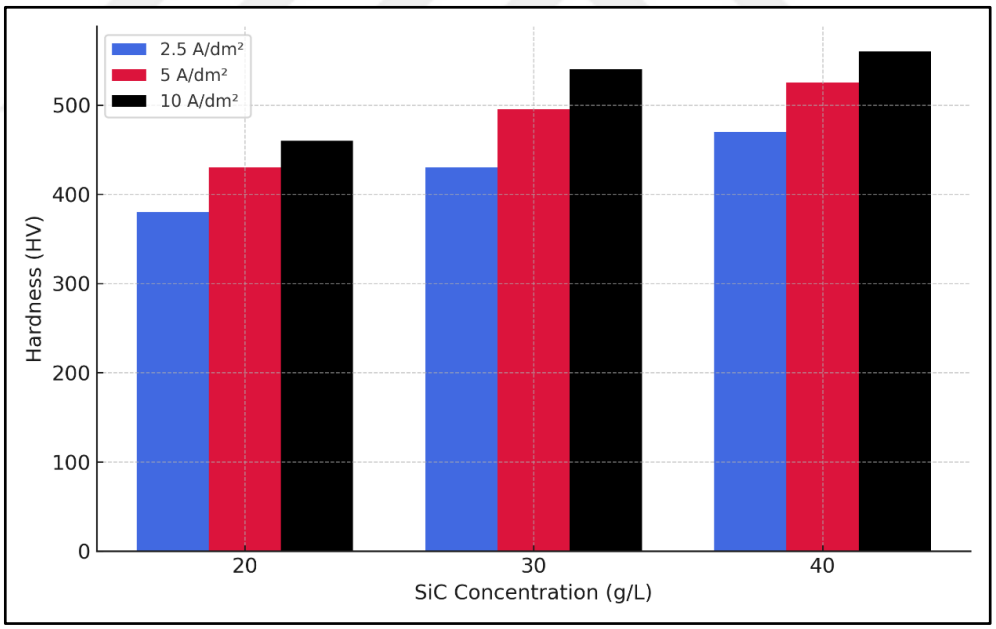


**Figure 4.11** Effect of SiC concentration and current density on the microhardness (HV) of Ni–SiC composite coatings.

Figure 4.11 shows the microhardness (HV) values of Ni–SiC composite coatings obtained under different SiC concentrations (20, 30, 40 g/L) and three different current densities (2.5, 5.0 and 10.0 A/dm²). When the graph is examined, it is clearly seen that

there is a significant increase in the hardness of the coating as both the SiC concentration and current density increase. At 20 g/L SiC concentration, the hardness values are around ~380 HV (2.5 A/dm²), ~430 HV (5 A/dm²) and ~460 HV (10 A/dm²), respectively; when 40 g/L is reached, these values increase to approximately ~470 HV, ~530 HV and ~560 HV. This situation shows that both more SiC particles are embedded in the nickel matrix and these particles are better integrated into the coating due to the increased current density. Especially the maximum hardness value obtained when the current density of 10 A/dm² and the SiC concentration of 40 g/L are combined reveals that this parameter combination provides the most suitable conditions.

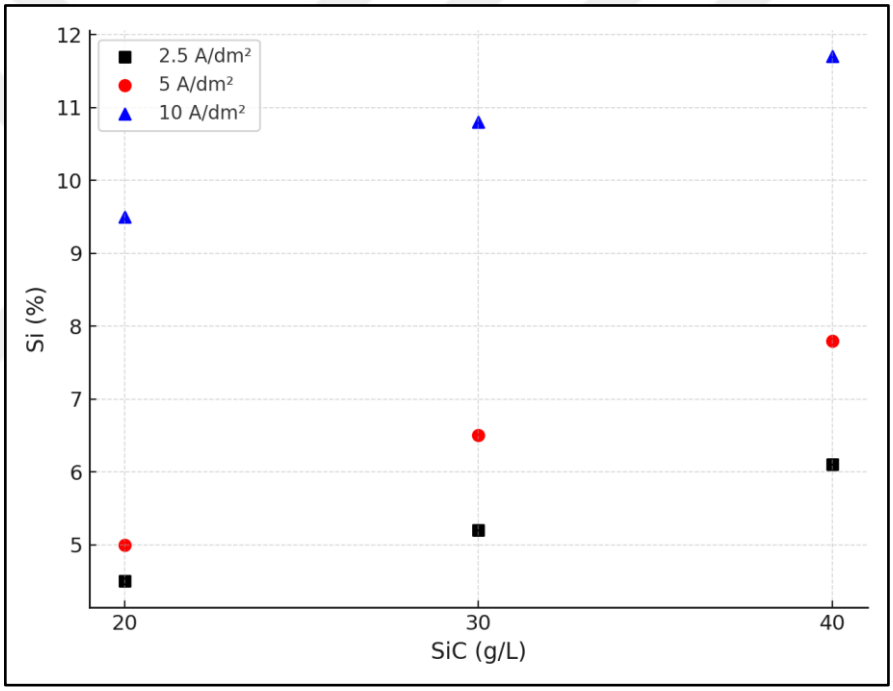


**Figure 4.12** Change in SiC incorporation in Ni-SiC coatings as a function of bath SiC concentration and current density.

Figure 4.12 shows the effect of the SiC concentration in the bath and the applied current density on the Si ratio in the coating. It is clearly seen that as the Si concentration increases, there is a significant increase in the Si ratio embedded in the coating. Especially at a current density of 10 A/dm², approximately 9.5% Si was obtained at a SiC concentration of 20 g/L; this value increased to 11% at 30 g/L and 11.7% at 40 g/L.

This situation shows that the high current density and the high SiC amount in the bath together increase the electrophoretic mobility of the particles and embed them more effectively in the matrix. At the same time, an increase was observed at lower current densities such as 2.5 A/dm² and 5 A/dm², but the obtained Si ratios were more limited. This reveals that the effect between current density and particle concentration plays a critical role in obtaining homogeneous and sufficient reinforcement in composite coatings.

## 4.4 Tribological Behavior of Ni–SiC Coatings

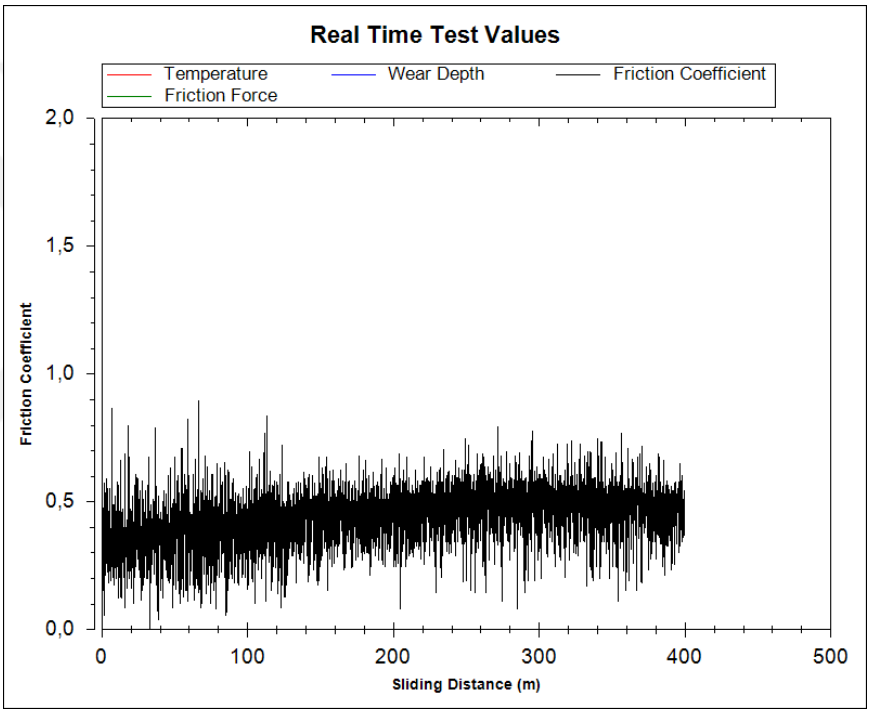


**Figure 4.13** Real-time friction coefficient (μ) variation with sliding distance for Ni–SiC coatings deposited at 2,5 A/dm² using an alumina counter ball. Both samples A were coated under identical conditions: pH 4.0, 55 °C, 75 min, 0.40 g/L SiC.

Figure 4.13 shows the friction test results for the coated sample at a current density of 2.5 A/dm². The test was performed using an alumina ($Al_2O_3$) ball, and the Coefficient of Friction (COF) formed over a certain sliding distance with the opposite surface was measured in real time.

In the graph, the coefficient of friction is observed to be 0.44 on average throughout

the test. Although slight fluctuations are observed in the first 50–100 meters, it is seen that the values become more stable in the following distances and no significant wear threshold occurs.

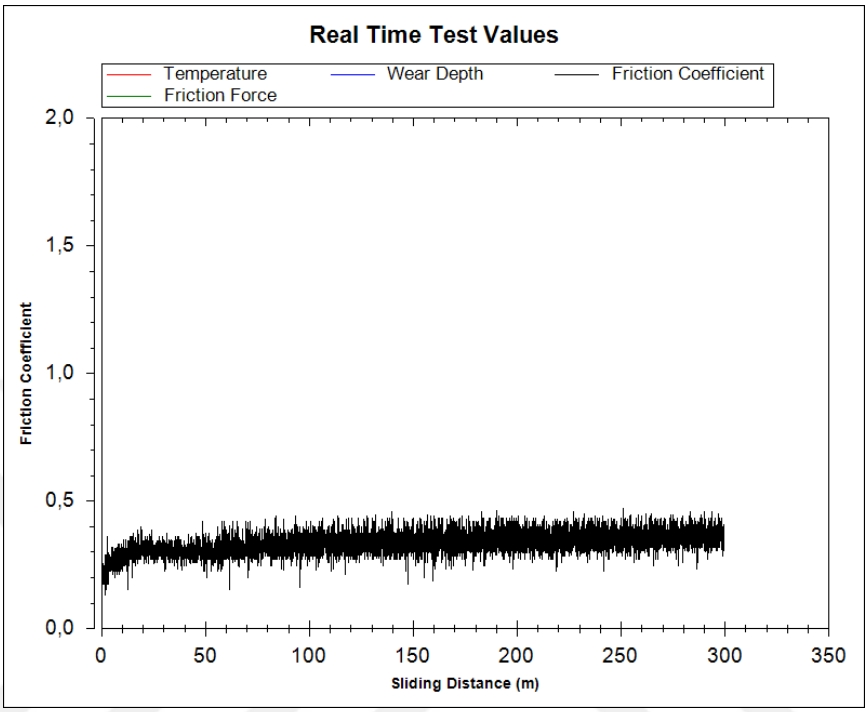


**Figure 4.14** Real-time friction coefficient (μ) variation with sliding distance for Ni–SiC coatings deposited at 5 A/dm² using an alumina counter ball. Both samples B were coated under identical conditions: pH 4.0, 55 °C, 75 min, 0.40 g/L SiC.

Figure 4.14 shows the real-time friction coefficient values of the friction test performed with alumina balls on the coated Ni/SiC surface at a current density of 5 A/dm². The graph shows that the friction coefficient reached a balance with a slight increase at the beginning of the test and stabilized in the range of approximately 0.35–0.45. These values are lower than the average friction coefficient obtained at 2.5 A/dm². This decrease can be attributed to the increase in the amount of SiC particles embedded during the coating. The increased SiC content creates a more homogeneous and hard surface layer, reduces the contact resistance during sliding and provides an improvement in the friction coefficient.

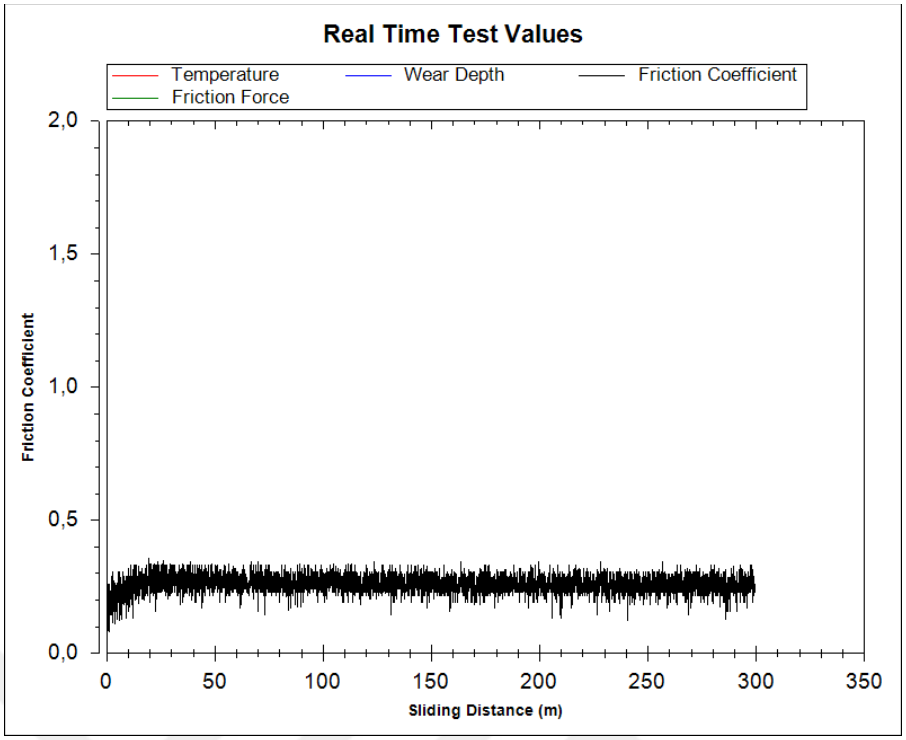


**Figure 4.15** Real-time friction coefficient (μ) variation with sliding distance for Ni–SiC coatings deposited at 10 A/dm² using an alumina counter ball. Both samples C were coated under identical conditions: pH 4.0, 55 °C, 75 min, 0.40 g/L SiC.

Figure 4.15 presents the real-time friction coefficient (μ) data of the friction test performed with alumina balls on the coated Ni-SiC surface under a current density of 10 A/dm². According to the results obtained, the friction coefficient remained constant at very low levels throughout the test, approximately in the range of 0.20–0.30. These values are lower than the COF values obtained at both 2.5 A/dm² and 5 A/dm² current densities. This decrease is directly related to the formation of a more compact and homogeneous microstructure at high current densities. In addition, the high rate of SiC particles integrated into the coating at this current level made the surface more resistant to wear. This minimized the friction formed on the contact surface.

The low fluctuation amplitude and stability in the graph indicate that the surface exhibited stable wear behavior and maintained its structural stability under the applied test conditions. In this context, 10 A/dm² stands out as the most efficient current density in terms of tribological performance.

## 4.5 Structural Phase Analysis via XRD

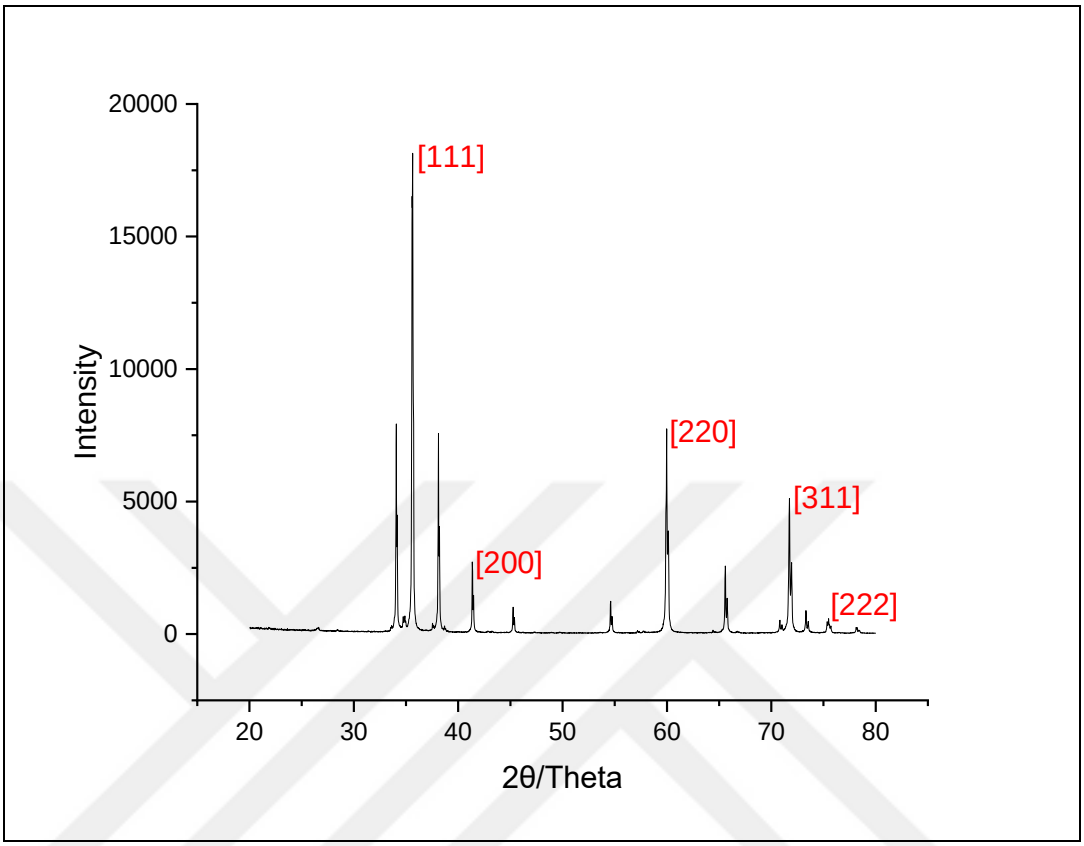


**Figure 4.16** XRD pattern of SiC ceramic powder (JCPDS No: 01-073-1663).

As a result of XRD analysis, the crystal structure of the SiC ceramic powder used was compared with the PDF card numbered 01-073-1663 and it was determined that the characteristic pattern of the β-SiC phase was formed. In the obtained diffraction pattern, the peaks corresponding to the (200), (220), (311) and (222) planes, especially the intense (111) peak located at approximately 35.6°, were clearly observed. This situation reveals that the powder exhibits a single-phase cubic crystal structure and contains a high level of crystallinity. Especially the high intensity of the peak belonging to the (111) plane indicates that there is preferential crystallographic orientation in this plane direction.

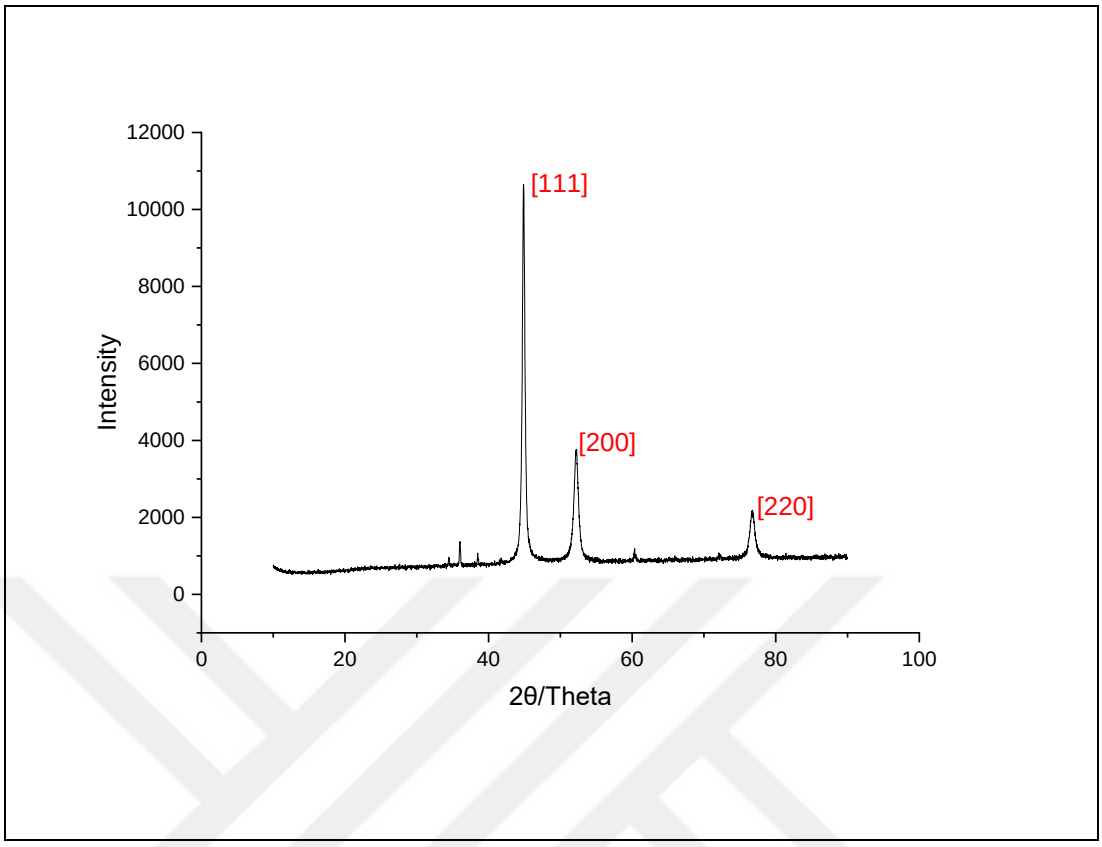


**Figure 4.17** XRD pattern of Ni/SiC coating deposited at 2.5 A/dm² for 75 min, showing dominant Ni peaks (JCPDS No: 01-071-4655) with no distinct SiC peaks (JCPDS No: 01-073-1663).

According to the XRD analysis of the coating obtained at a current density of 2.5 A/dm² for 75 minutes, it was observed that the structure was predominantly composed of nickel phase. The distinct diffraction peaks located at approximately 44.7°, 52.1° and 76.8° correspond to the (111), (200) and (220) planes of Ni, respectively, indicating that the coating is densely crystallized in the FCC crystal structure (JCPDS No: 01-071-4655). The fact that the characteristic peaks belonging to the ceramic powder added to the coating bath for SiC reinforcement cannot be clearly observed in this sample may be due to reasons such as low SiC ratio, inhomogeneous distribution or remaining in an amorphous structure. JCPDS No: 01-073-1663 card was used as a reference for the determination of the characteristic peaks belonging to the SiC phase. However, the dominant Ni phase in the general structure indicates that the crystal orientation occurs in the direction of the (111) plane.

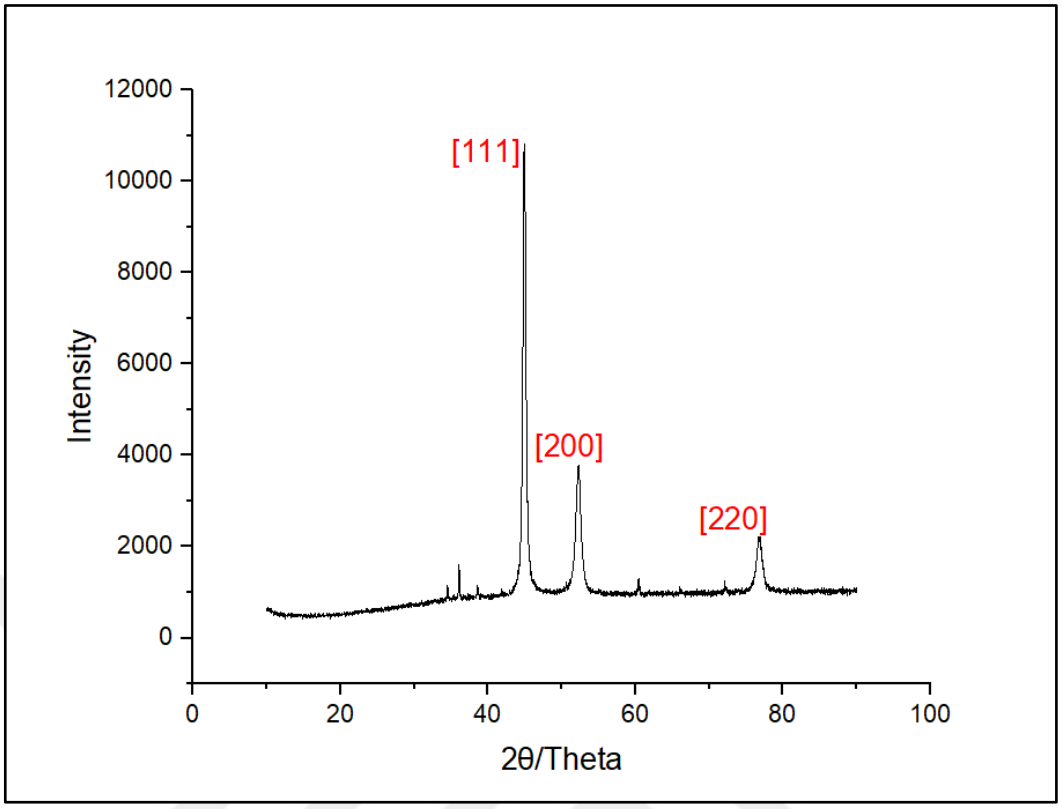


**Figure 4.18** XRD pattern of Ni/SiC coating obtained at 5 A/dm² for 75 minutes, showing peaks of Ni, SiC, and possible $Ni_3Si$ phases.

In the XRD analysis of the Ni/SiC composite coating obtained at a current density of 5 A/dm² for 75 minutes, the high intensity peaks around 44.7°, 52.1° and 76.8° correspond to the (111), (200) and (220) planes of nickel, respectively, indicating that the coating is dominantly crystallized on the crystalline nickel phase in the FCC structure (JCPDS No: 01-071-4655). The weak peaks observed around 35.7°, 38.2° and 41.5° belong to the SiC phase in the composite and correspond to the (101), (103) and (202) planes, respectively (JCPDS No: 01-073-1663). These peaks indicate that SiC is more prominently located in the crystal structure compared to the previous low current density samples.

In addition, some peaks around 35.9°, 44.8° and 52.2° correspond to the $Ni_3Si$ intermediate phase (JCPDS No: 00-006-0690), indicating that a new compound may have formed in the coating as a result of the interaction between nickel and SiC.

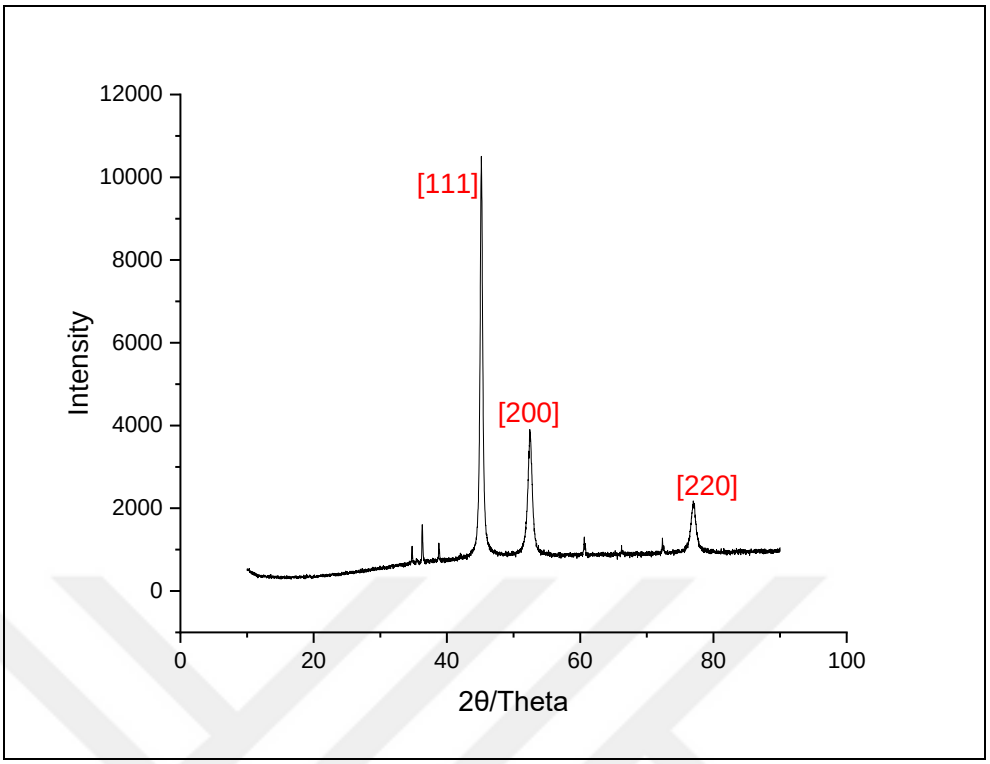


**Figure 4.19** XRD pattern of Ni/SiC coating obtained at 10 A/dm² for 75 minutes, showing distinct peaks of Ni and SiC phases (JCPDS No: 01-071-4655 and 01-073-1663).

In the XRD analysis of the Ni/SiC composite coating obtained as a result of electrodeposition performed at a current density of 10 A/dm² and for 75 minutes, the high intensity diffraction peaks observed at approximately 44.7°, 52.1° and 76.8° correspond to the (111), (200) and (220) planes of the FCC structured nickel phase, respectively (JCPDS No: 01-071-4655). This finding reveals that the coating contains a highly crystalline nickel matrix structure. When compared to the samples obtained at previous low current densities, it was determined that new and more distinct peaks appeared at around 35.7°, 38.2° and 41.5° in this coating. These peaks match the (101), (103) and (202) planes of the SiC phase (JCPDS No: 01-073-1663).

The clearer observation of diffraction peaks belonging to SiC due to the effect of increasing current density can be associated with the more effective embedding of ceramic particles into the coating structure and the more efficient operation of the co-deposition mechanism. This suggests that particle capture and integration into the matrix increase with the intensification of the electrochemical environment.

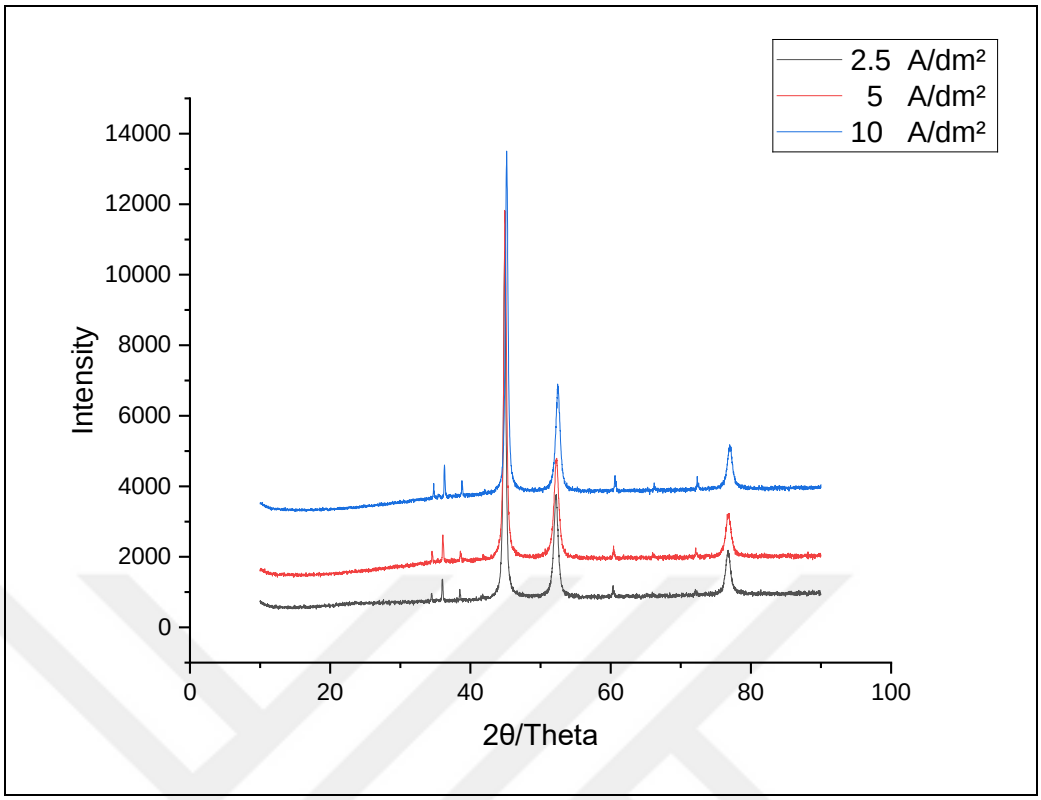


**Figure 4.20** Comparison of XRD patterns of Ni/SiC coatings deposited at 2.5, 5, and 10 A/dm² for 75 minutes. Increased current density enhances the visibility of SiC peaks.

The XRD patterns of Ni-SiC composite coatings produced for 75 minutes at different current densities (2.5, 5 and 10 A/dm²) are presented comparatively in Figure 4.17. The dominant peaks observed in all samples around 44.7°, 52.1° and 76.8° correspond to the (111), (200) and (220) planes of nickel, respectively, indicating that the coatings are built on the FCC structured crystalline nickel phase (JCPDS No: 01-071-4655).

While only the peaks belonging to the nickel phase were clearly observed at low current densities (2.5 A/dm²), it was observed that new pixels appeared in the range of 35–42° as the current densities increased (~5 and 10 A/dm²). These pixels belong to the SiC phase and are particularly compatible with the (101), (103) and (202) planes (JCPDS No: 01-073-1663). The increase in the intensity of these pixels belonging to SiC shows that the ceramic phase is more effectively incorporated into the coating structure at high current density.

# CHAPTER 5

## CONCLUSION

In this thesis, Ni-SiC electrocomposite coatings have been developed for surface properties enhancement of Al based piston engine cylinders for applications such as unmanned aerial vehicles (UAVs) where high wear resistance, light weight and thermal protection are of utmost importance. This work was motivated by a search for a green alternative to hexavalent chromium coatings, which pose substantial environmental and health hazards.

A full factorial experimental plan was performed for probing the effects of bath conditions (coating time, bath temperature, current density and SiC particles concentration) on coating quality. The coatings were prepared on 6061 aluminum substrates by EC deposition and studied in-depth for its structural, mechanical and tribological properties. The best coating deposition was found to be at current density of 10 A/dm, SiC concentration of 40 g/L at 55°C bath temperature and for the 75 minutes of deposition time. Under these conditions:

The thickness of the coating was about 165 μm, as observed by SEM cross-sectional imaging. Composite materials have been widely used for light weight and high strength applications. The microhardness of both composite layers was higher than 550 HV, which is the proof of the reinforcing effect of the SiC particles incorporated.

XRD analysis revealed the existence of Ni (111), (200) and (220) planes as well as the peaks characteristic for SiC at higher current densities, thus confirming the composite character.

Tribological analysis showed a considerable decrease in the friction coefficient from 0.44 (2.5 A/dm²) to 0.29 (10 A/dm²), which confirmed superior wear resistance and protective effect of the surface under the action of the sliding load.

These findings unambiguously indicate that Ni-SiC coatings developed at these optimized conditions possess higher structural integrity, mechanical strength, and

tribological properties as compared to coatings at lower applied current densities or particle concentrations.

The results of this study advance scientific knowledge of electrocoposition mechanism and particle collection efficiency and also indicate the industrial significance of Ni-SiC coatings in aerospace and high-performance applications. Subsequent works can examine the long-term wear behavior under cyclic loading, thermal fatigue performance, and the incorporation with hybrid coating systems to even broaden the potential uses of these advanced surface technologies.

# REFERENCES

[1] M. Gunston, *Development of Piston Aero Engines*, 2nd ed., Haynes Publishing, 2006.

[2] T. L. Schmitz and K. S. Smith, "An overview of reciprocating engines in UAV propulsion," Aerospace Science and Technology, vol. 52, pp. 1–10, 2016.

[3] J. B. Heywood, Internal Combustion Engine Fundamentals, 2nd ed., McGraw-Hill, 2018.

[4] A. Erdemir and J.-M. Martin, *Superlubricity*, Elsevier, 2007.

[5] C. Donnet and A. Erdemir, "Surface engineering for tribological applications," Wear, vol. 240, no. 2, pp. 210–219, 2000.

[6] TUSAŞ Engine Industries (TEI), "TEI-PG50 İki Zamanlı Benzinli Havacılık Motoru," TEI Resmî Web Sitesi, [Çevrimiçi].

[7] S. T. Oyama, The Chemistry of Transition Metal Carbides and Nitrides. Springer, 1996.

[8] B. Bhushan, Modern Tribology Handbook. CRC Press, 2000.

[9] C. Suryanarayana, Mechanical Alloying and Milling. Marcel Dekker, 2004.

[10] J. R. Davis, Ed., Surface Engineering for Corrosion and Wear Resistance. ASM International, 2001.

[11] P. Cavaleiro and J. T. M. De Hosson, Nanostructured Coatings. Springer Science & Business Media, 2006.

[12] D. R. Gabe, Principles of Metal Surface Treatment and Protection. Elsevier, 2014.

[13] M. Palaniappa and V. S. Raja, "Electrochemical deposition of Ni–SiC composite coatings and their properties," J. Appl. Electrochem., vol. 39, no. 12, pp. 2161–2169, 2009.

[14] M. F. Tabrizi, M. Aliofkhazraei, S. Z. Rahmani, and H. R. Rezaie, "Effect of pulse plating parameters on electrodeposition of Ni–SiC nanocomposite coatings," Surf. Coat. Technol., vol. 204, no. 6–7, pp. 1080–1085, 2010.

[15] H. Hu and Y. Wang, "Microstructure and wear properties of electrodeposited Ni–SiC composite coatings," J. Alloys Compd., vol. 461, no. 1–2, pp. 336–341, 2008.

[16] A. J. Bard and L. R. Faulkner, Electrochemical Methods: Fundamentals and Applications, 2nd ed., Wiley, 2001.

[17] Bard, L. R., & Faulkner, A. J., Introduction and overview of electrode processes. In Electrochemical Methods, (2nd. ed.) (2), United States of America: John Willey & Sons, Inc. 2001.

[18] Almeida, E. Surface treatments and coatings for metals. A general overview. 2. Coatings: Application processes, environmetal conditions during painting and drying, and new tendencies. In Am. Chem. Soc., 40 (15-20),16. 2001.

[19] Gamburg, Y. D., & Zangari, G. Introduction to electrodeposition: basic terms and fundamental concepts. In Theory and Practice of Metal Electrodeposition.

[20] Ulu, F. Electrochemical formation of brazing alloys on metal substrates. Middle East Technical University, 2014.

[21] Laboratory for Energy and Microsystems Innovation. (n.d.) Retrieved January 12, 2021, from http://web.mit.edu/lemi/rsc_electrokinetics.html/

[22] Bard, L. R., & Faulkner, A. J., Introduction and overview of electrode processes. In Electrochemical Methods, (2nd. ed.) (18), United States of America: John Willey & Sons, Inc. 2001.

[23] Bard, L. R., & Faulkner, A. J., Introduction and overview of electrode processes. In Electrochemical Methods, (2nd. ed.) (19), United States of America: John Willey & Sons, Inc. 2001.

[24] Paunovic, D. D., Schlesinger, M., & Synder, M. Fundamental considerations. In Modern Electroplating, (5th. ed.) (8), New Jersey: A John Wiley & Sons, Inc. 2010.

[25] Connection between Ecell, Gibbs free energy, and K. (n.d.) Retrieved January 14,2020,fromhttps://chem.libretexts.org/Bookshelves/Analytical_Chemistry/Supplemental_Modules_(Analytical_Chemistry)/Electrochemistry/Electrochemistry_and_Thermodynamics/

[26] Gamburg, Y. D., & Zangari, G. Introduction to electrodeposition: basic terms and fundamental concepts. In Theory and Practice of Metal Electrodeposition (9), London: Springer. 2011.

[27] Dını, J. W., & Snyder, D. D. Electrodeposition of copper. In Modern Electroplating, (5th. ed.) (50), New Jersey: A John Wiley & Sons, Inc. 2010.

[28] Paunovic, D. D., Schlesinger, M., & Synder, M. Fundamental considerations. In Modern Electroplating, (5th. ed.) (4), New Jersey: A John Wiley & Sons, Inc. 2010.

[29] Bard, L. R., & Faulkner, A. J., Kinetics of electrode reactions. In Electrochemical Methods, (2nd. ed.) (92), United States of America: John Willey & Sons, Inc. 2001.

[30] Paunovic, D. D., Schlesinger, M., & Synder, M. Fundamental considerations. In Modern Electroplating, (5th. ed.) (6), New Jersey: A John Wiley & Sons, Inc. 2010.

[31] Gamburg, Y. D., & Zangari, G. Introduction to electrodeposition: basic terms and fundamental concepts. In Theory and Practice of Metal Electrodeposition (19), London: Springer. 2011.

[32] Nickel Institute. Current Distribution. in Nickel Plating Handbook (10). 2014.

[33] NOVA SCIENCE IN THE NEWS, 2000, The Science and Technology of Composite Materials [Online], Austrailian Acedemy of Science, http://www.science.org.au/nova/059/059key.htm.

[34] SOY, E., 2009, Kompozit Malzemeler, Ders Notları, Sakarya Üniversitesi Teknoloji Fakültesi, Sakarya.

[35] WIELAGE, B., STEINHAUSER, S., HENKER, A., 1998, Manufacture and Properties of Composite Coatings: An Introduction, Journal of Thermal Sprey Technology, 8 (4), 512-516.

[36] ENŞİCİ, A., 2004, Polimer Esaslı Kompozit Malzemeler ve Ürün Tasarımında Kullanımları [Online], İstanbul teknik üniversitesi, Endüstüri Ürünleri Tasarımı Bölümü, http://www.turkcadcam.net/rapor/kompozit-malzemeler/ Tarihi: 6 Nisan 2010].

[37] PETERS, S. T., 1998, Introduction, Basics and Road Map, HandBook of Composites, Chapman & Hall, an imprint of Thomson Science, 2-6 Boundary Row, London, 1-20.

[38] STROUMBOULI, M., GYFTOU, P., PAVLATOU, E. A., SPYRELLIS, N., 2004, Codeposition of Ultrafine WC Particles in Ni Matrix Composite Electrocoatings, Surface & Coatings Technologhy, 195 (2-3), 325-332,

[39] MOUSTAFA, S. F., ABDEL-HAMID, Z., ABD-ELHAY, A. M., 2001, Copper Matrix SiC and Al2O3 Particulate Composites by Powder Metallurgy Technique, Materials Letters, 53 (4-5), 244-249.

[40] MUSIANI, M., 2000, Electrodeposition of Composites: an Expanding Subject in Electrochemical Materials Science, Electrochimica Acta, 45 (20), 3397-3402.

[41] BURZYNSKA, L., RUDNIK, E., KOZA, J., BLAZ, L., SZYMANSKI, W., 2007, Electrodeposition and Heat Treatmen of Nickel/Silicon Carbide Composites, Surface & Coatings Technology, 202 (12), 2545-2556.

[42] GYFTOU, P., STROUMBOULI, M., PAVLATOU, E. A., ASIMIDIS, P., SPRYLLIS, N., 2005, Tribological Study of Ni Matrix Composite Coatings Containing Nano and Micron SiC Particles, Electrochimica Acta, 50 (23), 4544-4550.

[43] BESRA, L., LIU, M., 2006, A Review on Fundamentals and Applications of Electrophoretic Deposition, Progress in Materials, 52, 1-61.

[44] WIKIPEDIA, 2005, Electrophoretic Deposition http://en.wikipedia.org/wiki/Electrophoretic_deposition [Online], [Ziyaret Tarihi: 25 Mayıs 2011].

[45] HACIALİOĞLU, H. İ., 2010, Kompozit Malzemeler Sektörü, [Online], Web, http://www.yapiveri.com/UzmanGozuyle/kompozit-malzemeler-sektoru 2014.html [Ziyaret Tarihi: 7 Mart 2010].

[46] HOVESTAD, A., JANSEN., J. J. L., 2005, Electroplating of Metal Matrix Composites by Codeposition of Suspended Particles, Modern Aspects of Electrochemistry, B.E. Conway et. al. Academic/Plenum, New York, 6-526.

[47] HU, F., CHAN, K. C., 2004, Electrodeposition Behaviour of Ni-SiC Composite Under Different Shaped Waveforms, Applied Surface Science, 233 (1-4), 163-171.

[48] LEE, H., LEE, H., JEON, J., 2008, Electrolytic Deposition Behaviours of Ni-SiC Composite Coatings Containing Submicron-Sized SiC Particles, Metals and Materials, 14 (5), 599-605

[49] LEE, H., LEE, H., JEON, J., 2006, Codeposition of micro and nano-sized SiC particles in the nickel matrix composite coatings obtained by electroplating, Surface & Coatings Technology, 201 (8), 4711-4717.

[50] HOU, K. H., GER, M. D., WANG, L. M., KE, S. T., 2002, The Wear Behaviour of Electro-codeposited Ni-SiC Composites, Wear, 253 (9-10), 994-1003.

[51] KUO, S., CHEN, Y., GER, M., HWU, W., 2004, Nano-Particles Dispersion Effect on Ni/Al2O3 Composite Coatings, Materials Chemistry and Physics, 86 (1), 5-10.

[52] LOW, C.T.J., WILLS, R.G.A., WALSH, F.C., 2006, Electrodeposition of Composite Coatings Containing Nanoparticles in a Metal Deposit, Surface and Coatings Technology, 201, 371-383.

[53] VAEZI, M. R., SADRNEZHAAD, S. K., NİKZAD, L., 2007, Electrodeposition of Ni-SiC Nano-Composite Coatings and Evaluation of Wear and Corrosion Resistance and Electroplating Characteristics, Colloids and Surfaces A: Physicoche. Eng. Aspects, 315 (1-3), 176-182.

[54] ARAN A., 2000, Metal Matrisli Kompozit Malzemeler, Ders Notları, İstanbul Teknik Üniversitesi Makina Fakültesi, İstanbul.

[55] GARCIA-LECINA, E., GARCIA-URRUTIA, I., DIEZ, J. A., SALVO, M., SMEACETTO, F., GAUTIER, G., SEDDON, R., MARTIN, R., 2008, Electrochemical Preparation and Characterization of Ni/SiC Compositionally Graded Multilayered Coatings, Electrochimica Acta, 54 (9), 2556-2562.

[56] HEIDARI, G., TAVAKOLI, H., MOUSAVI KHOLE, S. M., 2010, Nano SiC-Nickel Composite Coatings From a Sulfamat Bath Using Direct Current and Pulsed Direct Current, Journal of Materials Engineering and Performance, 18 (8), 1183-1188.

[57] KNOTE, A., KRÜGER, H. G., KUPS, T., KERN H., SPIESS, L., 2007, Metal-Ceramic Composite Layers on Stainless Steel Through the Combination of Electrophoretic Deposition and Galvanic Processes, Journal Material Science, 42 (12), 4545-4551.

[58] Celis, J. P., Roos, J. R., & Buelens, C. (2000). Fundamental aspects of composite electroplating. Surface and Coatings Technology, 125, 401–409. https://doi.org/10.1016/S0257-8972(99)00563-6

[59] Benea, L., & Dorneanu, P. P. (2007). The influence of current density and saccharin on SiC co-deposition in Ni matrix composite coatings. Hydrometallurgy,87, 105–112. https://doi.org/10.1016/j.hydromet.2007.01.012

[60] Guglielmi, N. (1972). “Kinetics of the deposition of inert particles from electrolytic baths.” *Journal of The Electrochemical Society*, 119(8), 1009–1012.

[61] Low, C. T. J., Wills, R. G. A., & Walsh, F. C. (2006). “Electrodeposition of composite coatings containing nanoparticles in a metal deposit.” *Surface and Coatings Technology*, 201(1-2), 371–383.